LA-UR-24-22842

Approved for public release; distribution is unlimited.

Title:	Preserving Superconvergence of Spectral Elements for Curved Domains
Author(s):	Jones, Jacob Taylor
Intended for:	These are the slides for my dissertation defense.
Issued:	2024-03-28

Preserving Superconvergence of Spectral Elements for Curved Domains

Jacob Jones

Department of Applied Mathematics and Statistics
Stony Brook University

April 5th, 2024

Outline

Introduction and Motivation

- Finite Element Methods (FEM) and Spectral Element Methods (SEM) are crucial for solving partial differential equations (PDEs) on complex geometries.
- SEM offers superior accuracy due to potential superconvergence for simple domains.
- Challenges persist for domains with curved boundaries, restricting SEM's advantages in real-world applications.

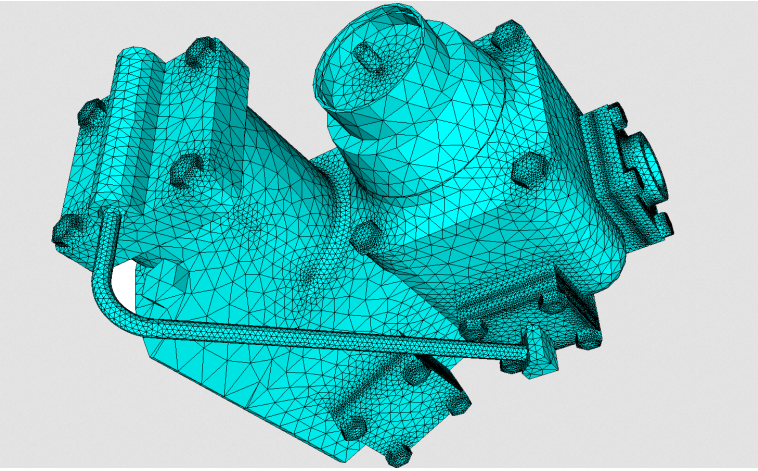

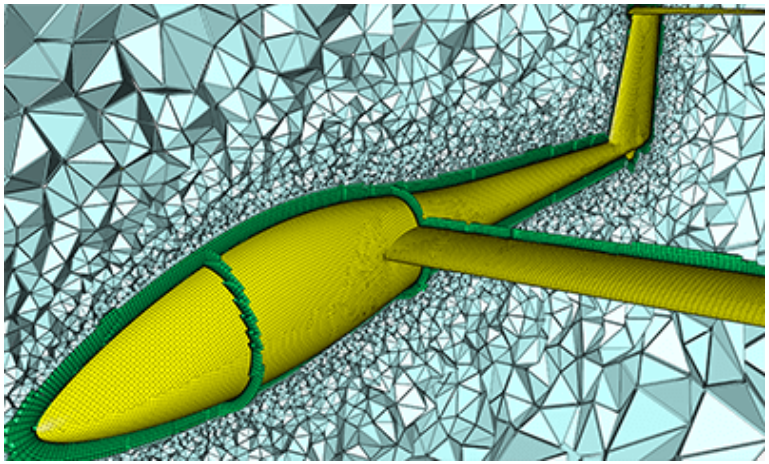

Proposed Solution

- Introduction of a novel strategy to enhance accuracy and maintain superconvergence of SEM in curved domains.
- Strategy includes a mesh-generation procedure with geometrically refined elements near curved boundaries and a post-processing phase using the Adaptive Extended Stencil Finite Element Method (AES-FEM).
- The method, named **A**ES-FEM **p**ost-processed **S**pectral **E**lement **M**ethod (ApSEM), aligns the accuracy of non-tensor-product elements with superconvergent spectral elements.

Contributions

- First demonstration of superconvergence over curved domains for both Dirichlet and Neumann boundary conditions in both 2D and 3D.
- Demonstration of the significant influence of geometric accuracy over the element shapes for FEM and SEM.
- Theory regarding the loss of superconvergence near curved boundaries.
- Demonstration of the efficiency of ApSEM, leveraging the surface-to-volume ratio.
- Presentation of a viable alternative to other discretization methods that rely on exact geometries.

Outline

FEM Formulation

- Principles expressed through the n-dimensional elliptic boundary value problem:

$$\mathcal{L}(u) \equiv -\nabla \cdot (c(x)\nabla u) = f(x),\ x \in \Omega^n \subset \mathbb{R}^n$$
$$u = p \text{ on } \Gamma_D^n$$
$$\frac{\partial u}{\partial n} = q \text{ on } \Gamma_N^n,$$

- n is the number of dimensions, typically $n = 2, 3$.
- The domain Ω^n is smooth and simply connected with boundary Γ^n.
- Boundary conditions combine Dirichlet conditions on Γ_D^n and Neumann conditions on Γ_N^n.

Mesh and Finite Element Space

- The domain Ω^n is approximated by a partition $\mathcal{T}^n$:

$$\mathcal{T}^n = \left\{ \bigcup_{i=1}^{E} \tau_i \middle| \, \forall \tau_i, \tau_j \quad \tau_i \cap \tau_j = \emptyset \text{ if } i \neq j \right\}.$$

- $\mathcal{T}^n$ is a mesh.
- Elements are in general n-dimensional simplexes or parallelotopes.
- Additional nodes define higher-degree elements.

Finite Element Spaces

- $P_k^n(\tau_i)$: polynomials of degree $\leq k$ on τ_i.
- n-dimensional degree k Lagrange space:

$$\mathbb{P}_k^n = \left\{\phi \in C^0(\Omega^n) | \phi(\tau_i) \in P_k^n(\tau_i), \forall \tau_i \in \mathcal{T}\right\}.$$

- Tensor-product space for n-dimensional parallelotopes:

$$\mathbb{Q}_k^n = \bigotimes_{i=1}^{n} \mathbb{P}_k^1.$$

- Approximation of u in trial space $\mathcal{U}$:

$$u \approx u_h = \sum_{i=1}^{N} U_i \phi_i, \ \phi_i \in \mathcal{U}.$$

- U_i: unknown coefficients, ϕ_i: trial functions.

Galerkin Formulation

$$\underbrace{\int_{\Omega^n} (c(x)\nabla u_h) \cdot \nabla v \, d\Omega^n}_{a(u_h,v)} = \underbrace{\int_{\mathcal{T}^n} f(x) v \, d\Omega^n}_{L(v)}.$$

- Gives an $M \times N$ linear system from Green's identity:

$$\boldsymbol{K}\boldsymbol{u} = \boldsymbol{f}.$$

- $\boldsymbol{u}$: vector composed of unknown U_i, $\boldsymbol{K}$: stiffness matrix, $\boldsymbol{f}$: load vector.
- Galerkin formulation when $\mathcal{V} = \mathcal{U}$.
- Bilinear form of the equation:

$$a(u_h, v) = L(v).$$

Spectral Element Method (SEM)

- Same formulation and assembly as FEM.
- Uses high-order Lagrange polynomials as basis functions with lobatto node distribution.
- Lagrange polynomials can be used to construct basis using any set of points (Generalized Lagrange Polynomials).

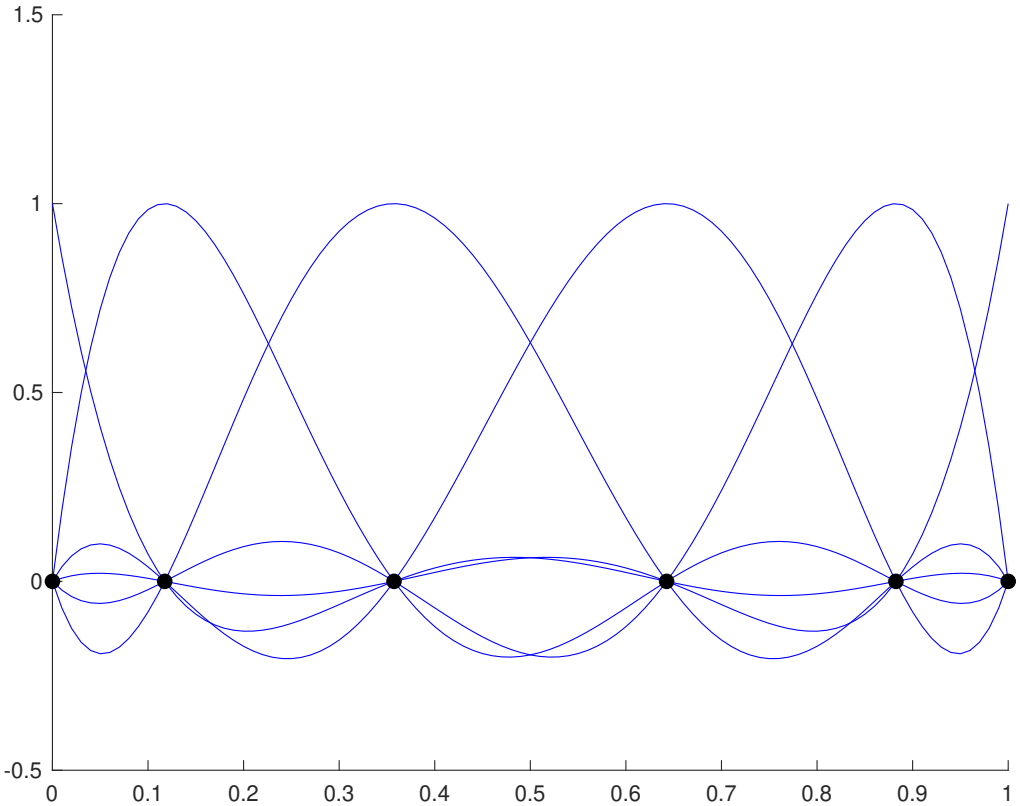

Figure: Degree 5 Lagrange polynomials using gauss-lobatto points.

Isogeometric Analysis (IGA)

- IGA[1] combines FEM and NURBS-based CAD.
- Handles curved boundaries directly.
- Uses same functions for CAD geometry and FEM fields.
- Uses NURBS or T-splines for geometry, trial space, and test space.

$$N_{i,p}(\xi) = \frac{\xi - \xi_i}{\xi_{i+p} - \xi_i} N_{i,p-1}(\xi) + \frac{\xi_{i+p+1} - \xi}{\xi_{i+p+1} - \xi_{i+1}} N_{i+1,p-1}(\xi),$$

$$R_{i,p}(\xi) = \frac{w_i N_{i,p}(\xi)}{\sum_{j=1}^{n} w_j N_{j,p}(\xi)}.$$

- IGA limitations:
  - Local mesh refinement is complex.
  - Larger patch influence leads to denser stiffness matrix and higher computational cost.

[1] Hughes, Cottrell, and Bazilevs, *Comput. Methods. Appl. Mech. Eng.* (2005).

NURBS Enhanced Finite Element Method (NEFEM)

- NEFEM[2] is a middle ground of FEM and IGA.
- NURBS for boundary, Lagrange polynomials for interior.
- Uses standard FEM meshes and trial functions.
- Adjusts quadrature rules and stiffness matrix for NURBS.
- Our workflow is simpler than NEFEM:
  - Use geometric reconstructions. No need for a CAD model.
  - Easier 3D implementation.
  - Applies techniques to recover superconvergence.

[2] Sevilla, Fernández-Méndez, and Huerta, *Int. J. Numer. Methods. Eng.* (2011).

Outline

Stability of the Finite Element Method

- Stability of finite element method is ensured by well-posedness of the variational problem, established via the Lax-Milgram theorem[3].

Theorem (Lax-Milgram Theorem)

Let H be a Hilbert space, $a(\cdot,\cdot)$ a bilinear form, and $L(\cdot)$ a linear functional on H. If $a(\cdot,\cdot)$ is continuous and coercive, and $L(\cdot)$ is continuous, then there exists a unique $u \in H$ such that

$$a(u,v) = L(v) \quad \forall v \in H.$$

- Continuity in the bilinear form and the linear functional ensures stability.
- Coercivity of the bilinear form ensures existence and uniqueness of the solution.

[3] Lax and Milgram, *Contributions to the Theory of Partial Differential Equations.(AM-33)* (1954).

Banach-Nečas-Babuška Theorem

- The Banach-Nečas-Babuška theorem[4] generalizes the Lax-Milgram theorem to Banach spaces.

Theorem (Banach-Nečas-Babuška Theorem)

Let W be a Banach space, V a reflexive Banach space, and $L(v) \in V^*$ the dual space of V. The variational problem is well-posed if and only if:

$$\exists \alpha > 0, \inf_{w \in W} \sup_{v \in V} \frac{a(w,v)}{\|w\|_W \|v\|_V} \geq \alpha$$

$$\forall v \in V, (\forall w \in W, a(w,v) = 0) \rightarrow (v = 0)$$

- This theorem is the basis for stability analyses like the Ladyzhenskaya-Babuška-Brezzi condition.

[4] Nečas, *Annali della Scuola Normale Superiore di Pisa-Scienze Fisiche e Matematiche* (1962); Babuška, *The Mathematical Foundations of the Finite Element Method with Applicaions to Partial Differential Equations* (1972).

Energy Norm and Céa's Lemma

- The *energy norm* is defined as:

$$\|u\|_E = \sqrt{\int_{\Omega^n} c(x)\nabla u \cdot \nabla u \, dx} = \sqrt{a(u,u)}.$$

- For constant $c(x) = \kappa$, it simplifies to $\|u\|_E = \|\nabla u\|_{L^2}$,
- Céa's lemma gives us:

$$\|u_h - u\|_E \leq \|u - v\|_E.$$

where u_h is the solution to the Galerkin formulation and v is an interpolation of u within the test space $\mathcal{U}$.

Error Estimation and Superconvergence

- The error estimation for an interpolation of u of degree k is:

$$\|\nabla v - \nabla u\|_{L^p} \leq C\|D^{k+1}u\|_{L^p}\mathcal{O}(h^k).$$

- The error in the energy norm is:

$$\|u_h - u\|_E = \mathcal{O}(h^k).$$

- Using the Aubin-Nitsche duality argument the error estimate in the L^2-norm is:

$$\|u_h - u\|_{L^2} = \mathcal{O}(h^{k+1}).$$

- Superconvergence for elliptic problems is defined as:

$$\|u_h - u\|_{\ell_2} = \mathcal{O}(h^{k+1+\alpha})$$

  where $\alpha > 0$.

- Gauss-Lobatto points converge at $\mathcal{O}(h^{k+2})$.[5]

[5] C. Chen, *Int. J. Numer. Anal. Model.* (2005).

Loss of Superconvergence

- We study SEM with curved boundary.
- Loss of superconvergence is due to the loss of orthogonality in Lagrange basis functions, $\phi_i(\boldsymbol{\xi}(\boldsymbol{x}))$.
- $\boldsymbol{\xi}(\boldsymbol{x})$ is the inverse mapping of $\boldsymbol{x}(\boldsymbol{\xi}) = \sum_{k=1}^{n_e} \boldsymbol{x}_k \varphi_k(\boldsymbol{\xi})$.
- $\boldsymbol{\xi}(\boldsymbol{x})$ is affine for linear basis functions and nonlinear for higher-order ones.
- This nonlinearity leads to orthogonality loss and superconvergence loss, assuming no other source of error cancellation.

Outline

ApSEM Overview

- Mesh using tensor-product elements and geometric refinement.
- Solving the PDE using SEM.
- Post-processing the solution using AES-FEM on a subdomain.
- Schwarz iteration to converge to a solution.

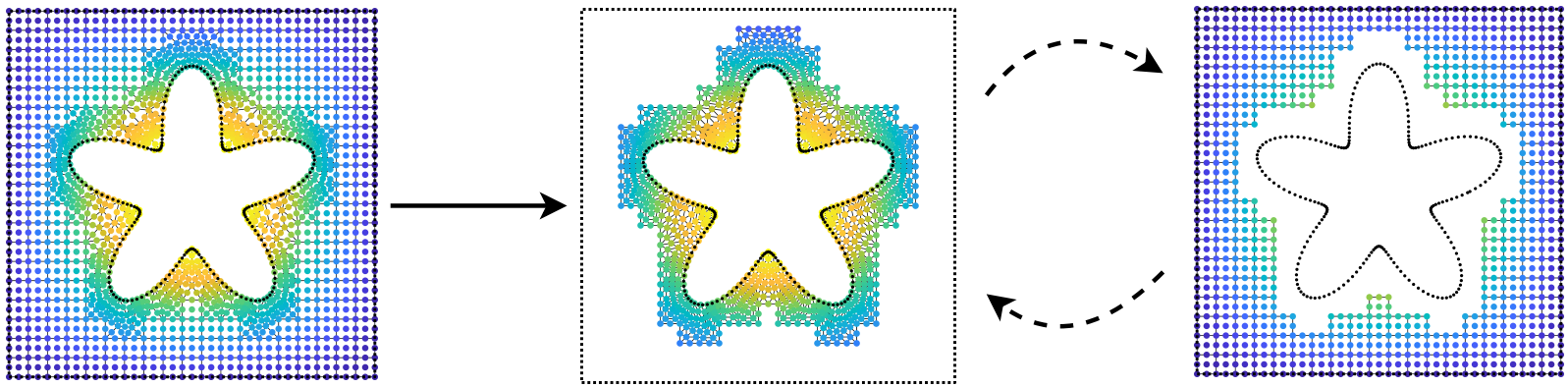

Step 1. Find the solution using SEM on the whole domain

Step 2. Find the solution using AES-FEM on a subdomain

Step 3 (Optional). Find the solution using SEM on a subdomain. Iterate with step 2

Figure: Workflow of ApSEM showing the subdomain where we apply AES-FEM and optionally the alternating Schwarz iteration to improve the solution.

Weighted Least Squares: Overview

- Weighted least squares approximates high-order function values and derivatives.
- Taylor series is used for high order approximation.
- Coefficients are determined by solving a generalized Vandermonde system.
- The weighting matrix assigns weights based on distances to the stencil center.

$$\boldsymbol{V} = \begin{bmatrix} 1 & x_1 - x_0 & y_1 - y_0 & (x_1 - x_0)^2 & \dots & (y_1 - y_0)^p \\ 1 & x_2 - x_0 & y_2 - y_0 & (x_2 - y_0)^2 & \dots & (y_2 - y_0)^p \\ & \vdots & & \vdots & & \vdots \\ 1 & x_m - x_0 & y_m - y_0 & (x_m - x_0)^2 & \dots & (y_m - y_0)^p \end{bmatrix}$$

Weighting Schemes

- Weighting function selection is crucial for approximation accuracy.
- Inverse distance weighting excels near curved boundaries:

$$\omega_i = \frac{\gamma_i}{\left(\sqrt{\|\boldsymbol{x}_i - \boldsymbol{x}_0\|_2^2 + \epsilon}\right)^{p/2}}$$

- Scaled Buhmann weights, based on radial basis functions[6], ensure high accuracy and error cancellation for interior mesh points:

$$\omega_i = \gamma_i \phi\left(\frac{\|\boldsymbol{x}_i - \boldsymbol{x}_0\|_2}{\rho}\right),$$

where

$$\phi(r) = \begin{cases} \frac{112}{45} r^{9/2} + \frac{16}{3} r^{7/2} - 7r^4 - \frac{14}{15} r^2 + 1/9 & \text{if } 0 \le r \le 1 \\ 0 & \text{if } r > 1. \end{cases}$$

- γ_i is for safegaurding against "short-circuiting" on surfaces.

[6] Buhmann, *Acta Numer.* (2000); Buhmann, *Math. Comput.* (2001).

AES-FEM and GLP Basis Functions

- AES-FEM uses Generalized Lagrange Polynomials (GLP) as basis functions.
- GLP basis function are constructed using weighted least squares.
  - As in Lagrange interpolation, function values serve as coefficients associated with GLP basis functions.
  - Approximate a function f to $k+1$st order for degree k polynomials.
  - Satisfy the partition of unity ($\sum_i \phi_i = 1$).

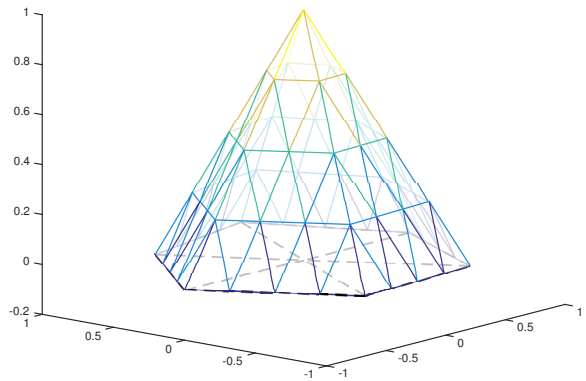

(a) Linear FEM Basis Function

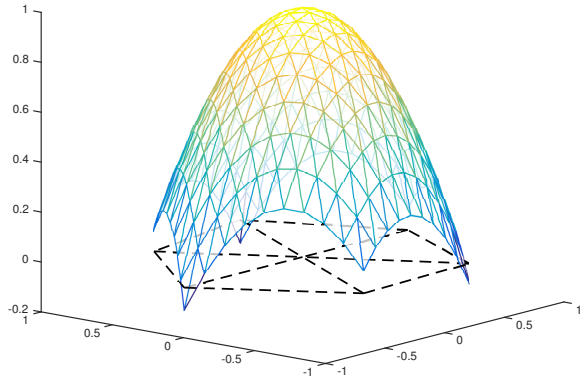

(b) Quadratic GLP Basis Function

Schwarz Iterations

$$\mathcal{L}(u_1^{k+1}) = f(x) \text{ in } \Omega_1$$
$$u_1^{k+1} = u^k \text{ on } \Gamma_1$$
$$u_1^{k+1} = p \text{ on } \partial\Omega_1/\Gamma_1$$

and

$$\mathcal{L}(u_2^{k+1}) = f(x) \text{ in } \Omega_2$$
$$u_2^{k+1} = u^k \text{ on } \Gamma_2$$
$$u_2^{k+1} = p \text{ on } \partial\Omega_2/\Gamma_2.$$

The final iteration is defined as

$$u^{k+1} = \begin{cases} u_1^{k+1} & \text{if } x \in \Omega_1 \\ u_2^{k+1} & \text{if } x \in \Omega/\Omega_2. \end{cases}$$

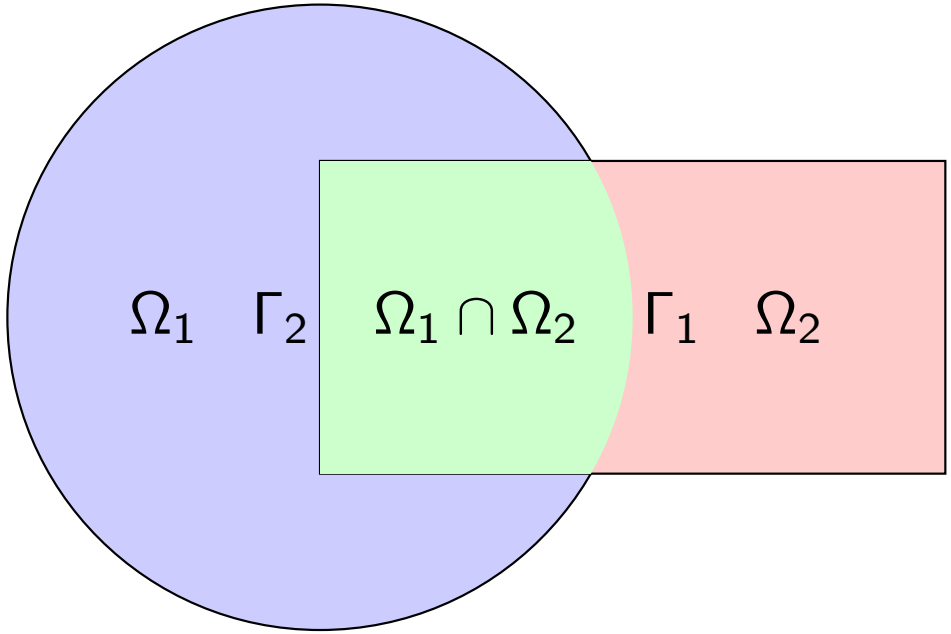

Figure: Demonstration of a domain while using the Schwarz alternating method. The domain Ω is decomposed into two subdomains Ω_1 and Ω_2. The intersection of the two subdomains is $\Omega_1 \cap \Omega_2$. The boundary of Ω_1 in $\Omega_1 \cap \Omega_2$ is Γ_1 and the boundary of Ω_2 in $\Omega_1 \cap \Omega_2$ is Γ_2.

Schwarz Iterations Convergence

Proposition (Convergence of Schwarz iterations using FEM/SEM)

Given a domain Ω partitioned into two overlapping subdomains Ω_1 and Ω_2, the Schwarz alternating iteration converges under mesh refinement when both subdomains use either finite elements or spectral elements to solve Linear elliptic PDEs.

- Corollary of Theorem I.1 in Lions[7].
- Believe the convergence can be generalized to SEM and AES-FEM using GWR framework.

[7] Lions (1988).

Stencil Selection for Interior Points

- Stencil selection for interior points is based on the ring size notation.
- Ring sizes correspond to different degree GLP basis functions.
- A full ring extension includes all elements connected to the existing nodes in the stencil.

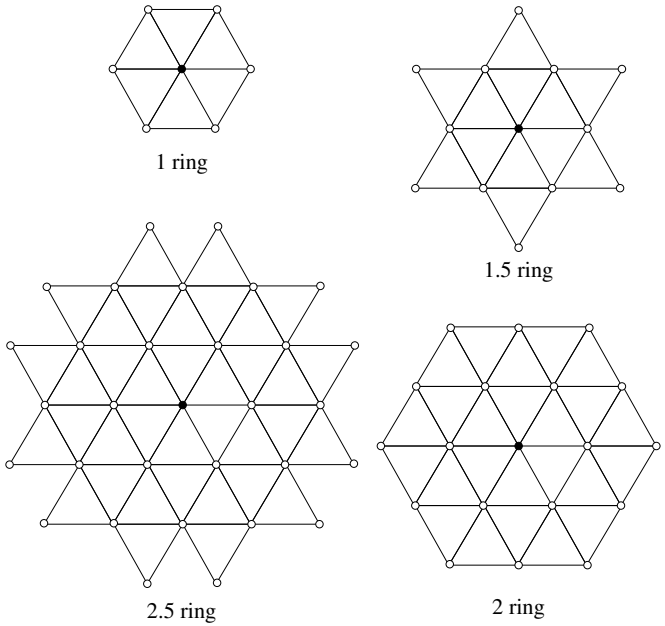

Figure: Examples of 2D stencils with 1-ring, 1.5-ring, 2-ring, and 2.5-ring neighborhoods of center node (in solid black).

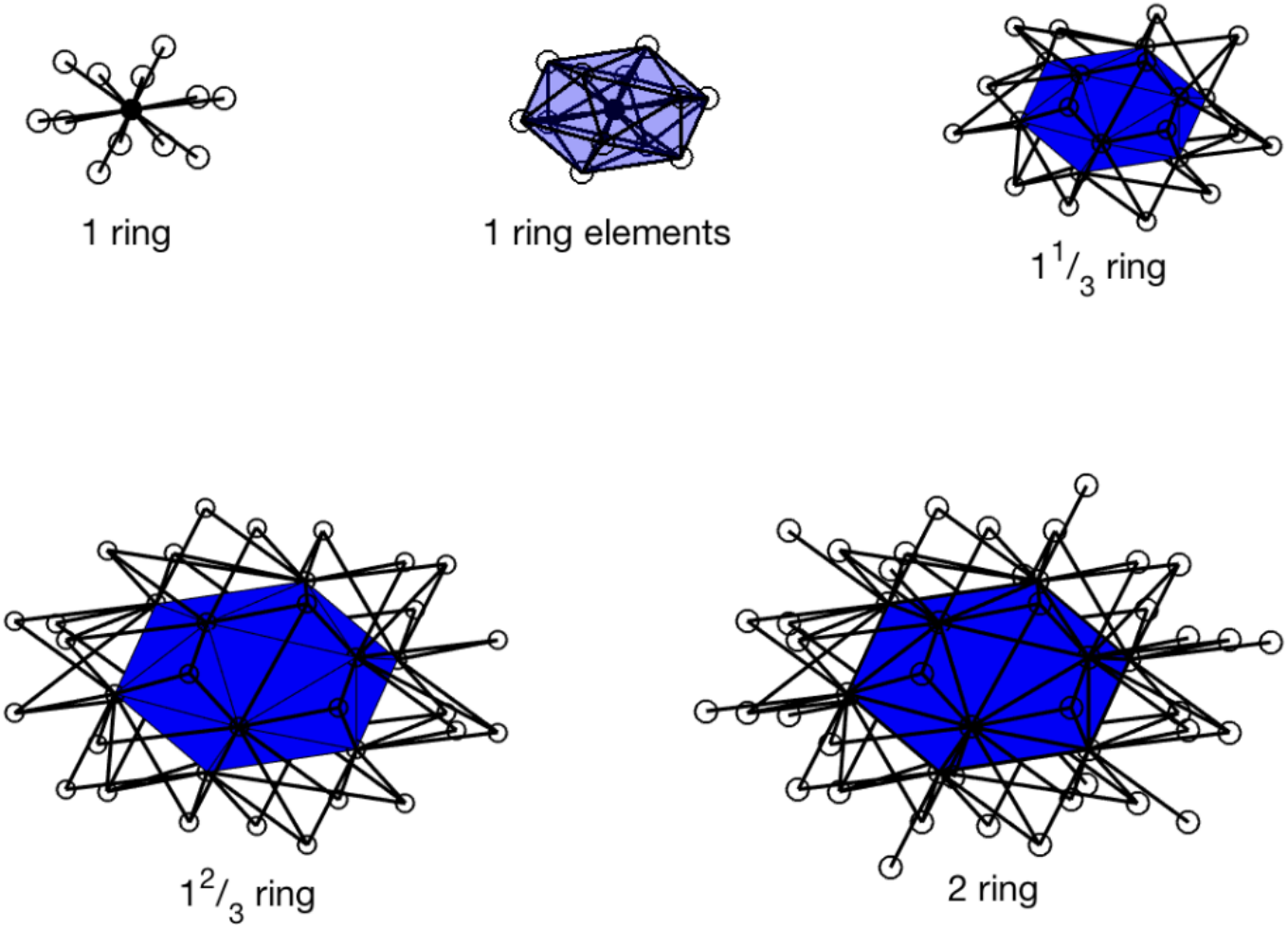

Figure: Examples of 3D stencils with 1-ring, $1\frac{1}{3}$-ring, $1\frac{2}{3}$-ring, and 2-ring neighborhoods of center node.

Overview of Mixed-Element Mesh Generation for ApSEM

- Mixed-element meshes are generated using tensor-product elements in the domain interior and unstructured elements near curved boundaries.

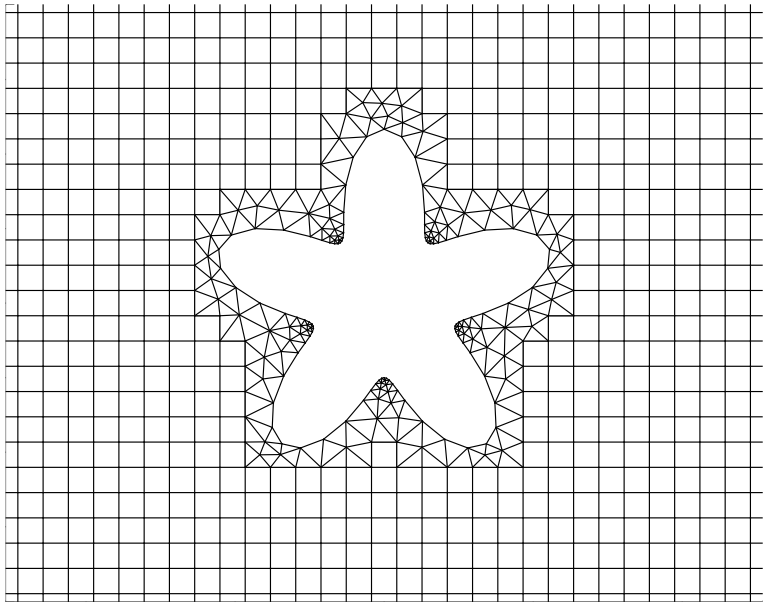

Figure: 2D mesh

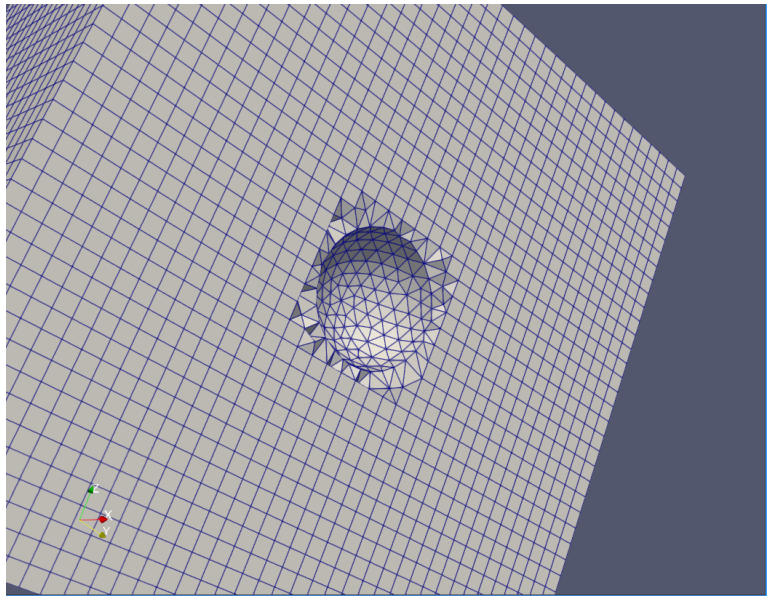

Figure: 3D mesh

Mesh Generation Steps in 2D - Step 1

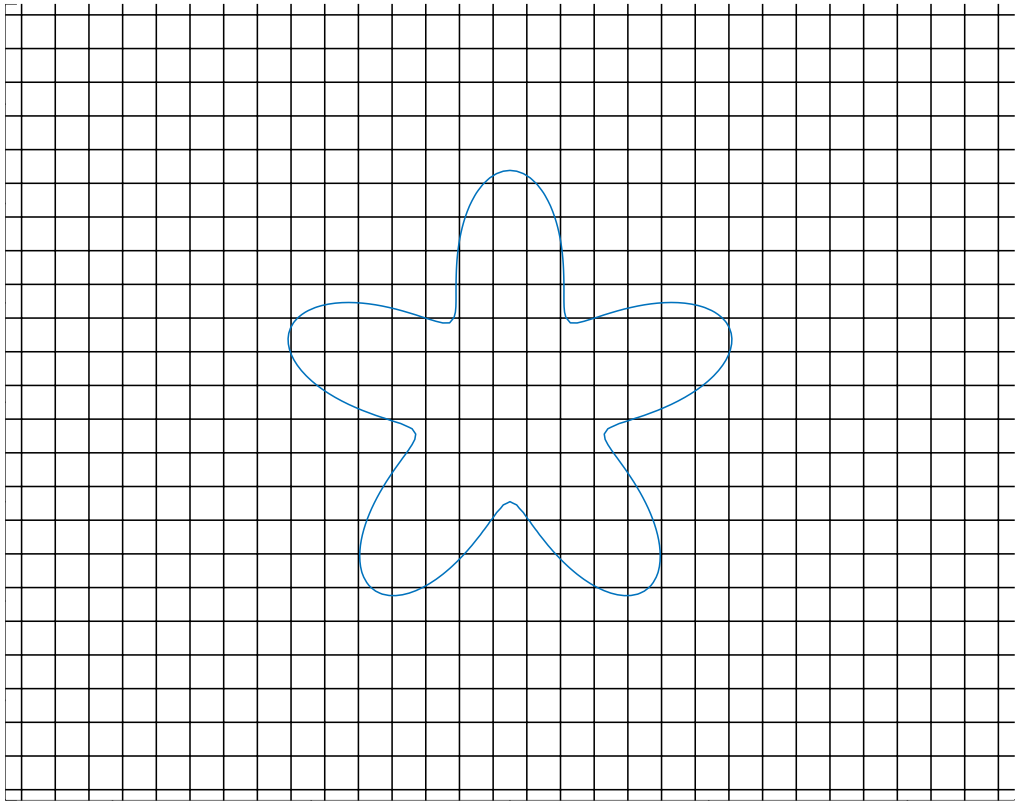

Figure: Initial structured mesh and curved boundary Γ

Mesh Generation Steps in 2D - Step 2

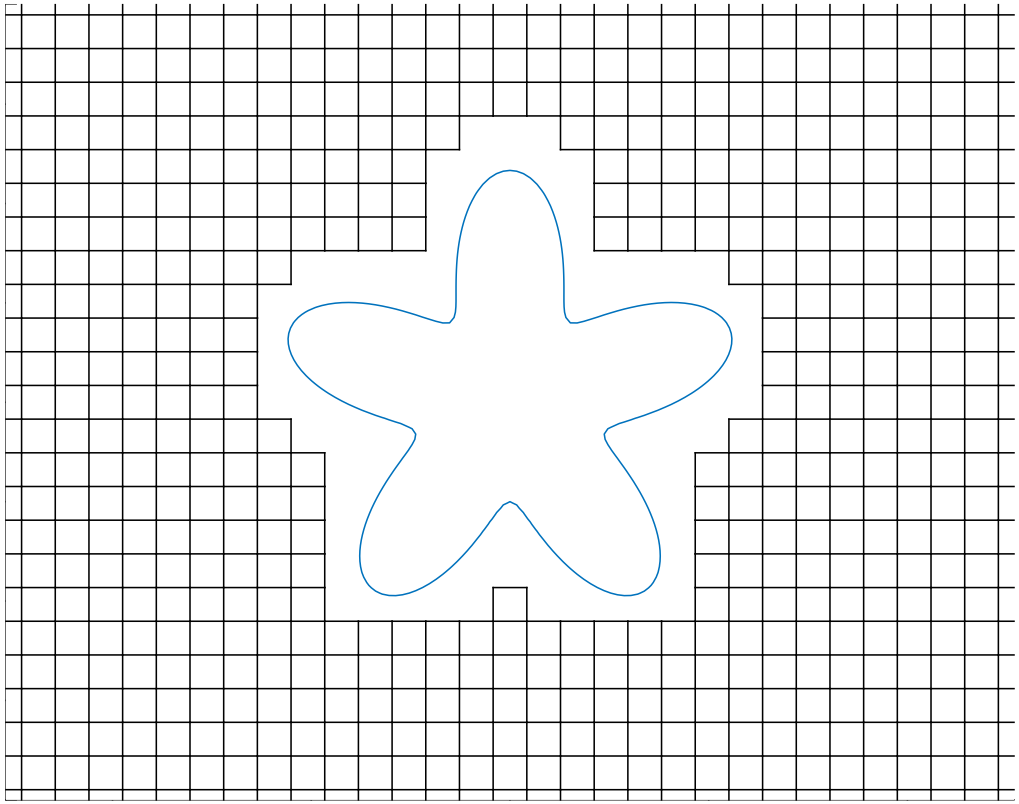

Figure: After removing elements outside or on Γ

Mesh Generation Steps in 2D - Step 3

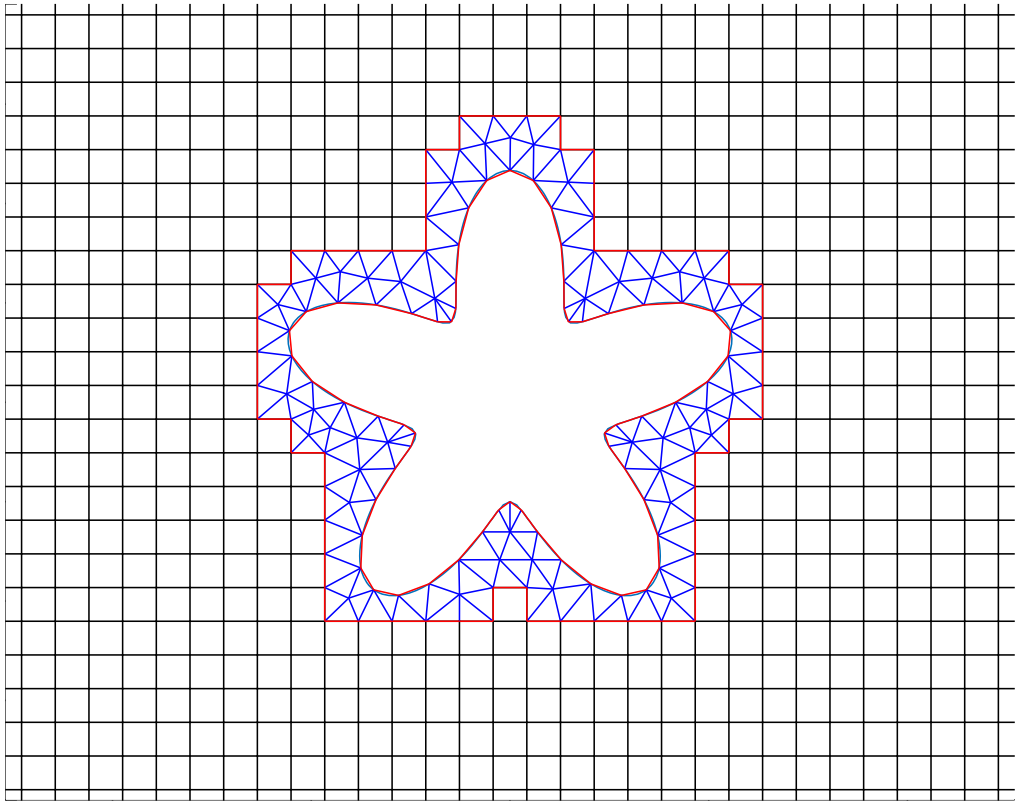

Figure: After generating conformal triangles

Mesh with and without h-GR adaptivity

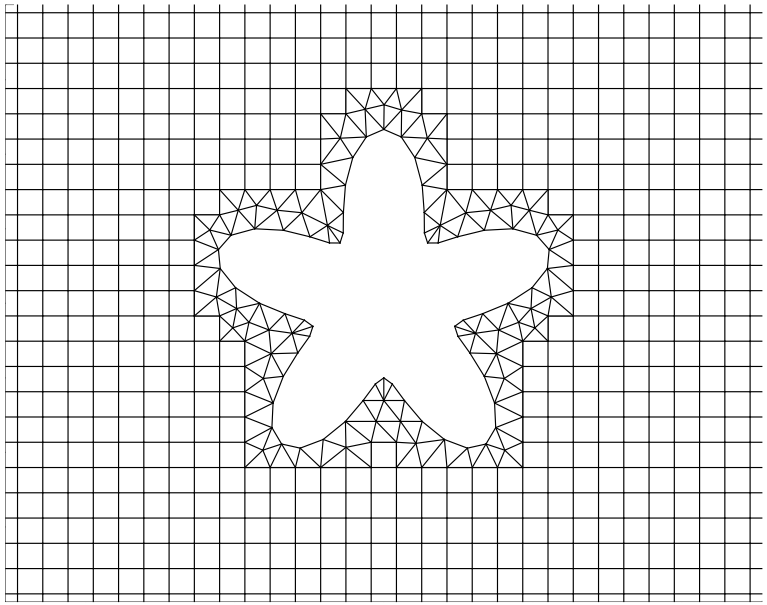

Figure: Mesh without h-GR

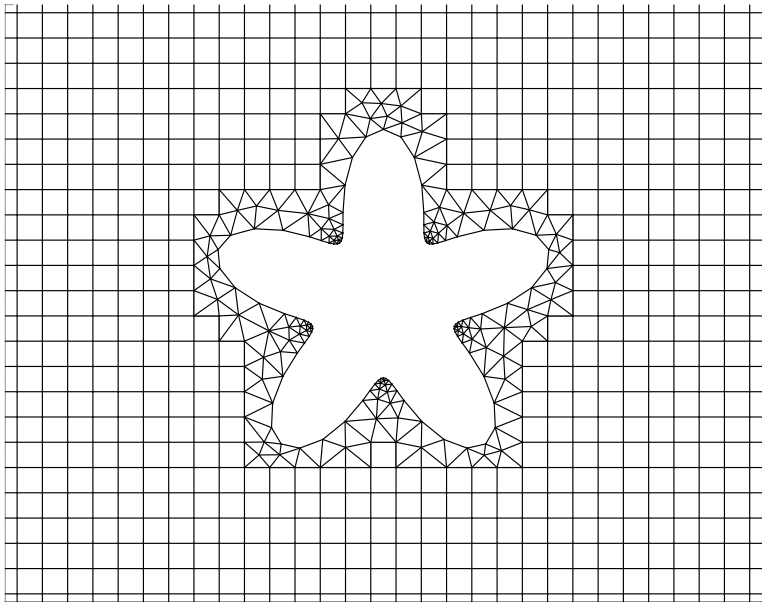

Figure: Mesh with h-GR

Example of an Extracted Near-Boundary Mesh

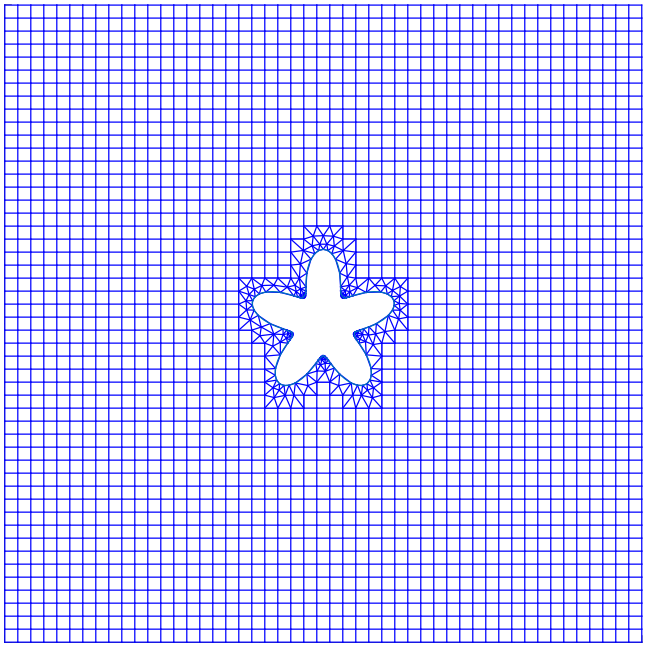

Figure: Quadratic mesh before splitting elements near the boundary

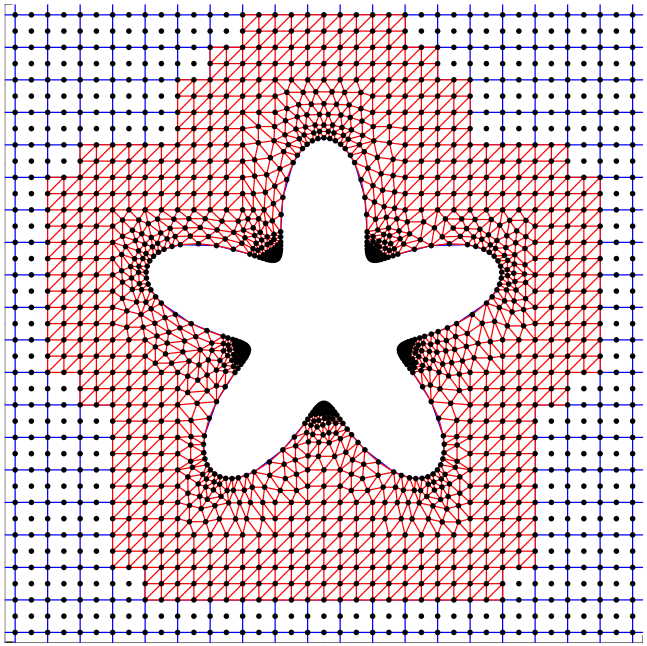

Figure: AES-FEM boundary mesh after extraction and splitting

3D Mixed Mesh Generation

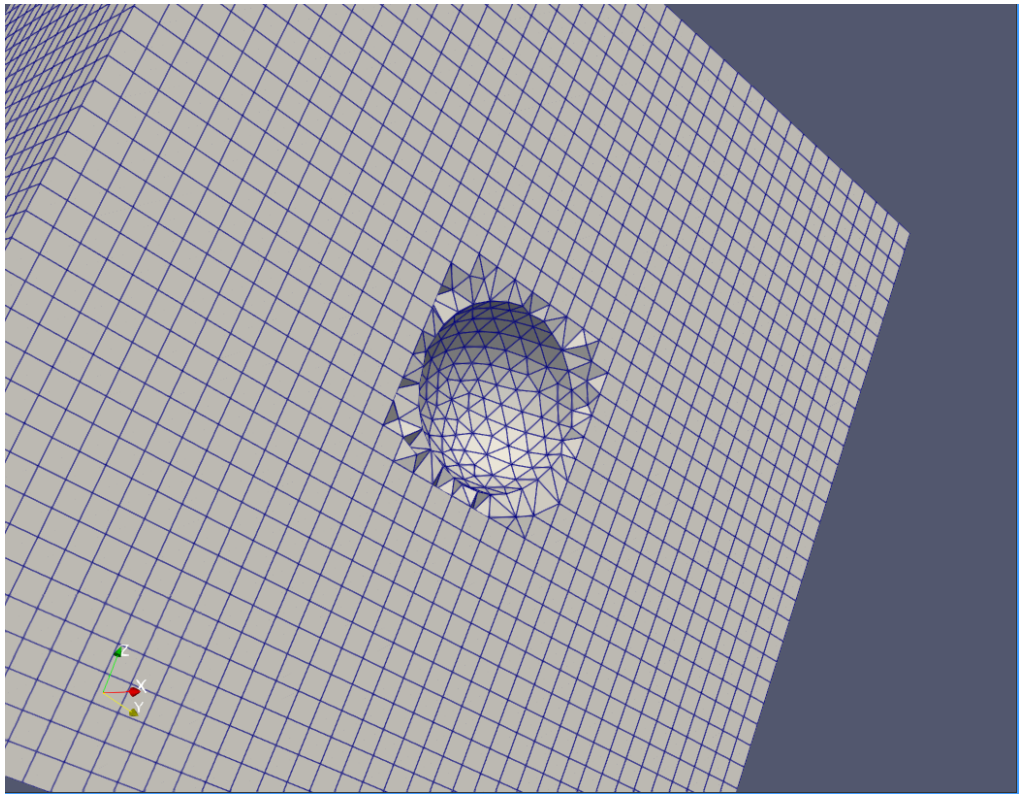

Figure: Illustration of the three-dimensional mixed mesh generation process applied to a domain with a spherical hole. The mesh is composed of tetrahedral elements near the curved boundary, and pyramidal/hexahedral elements in the exterior.

Implementation Details

- AHF[8] mesh data structure is used to store element adjacency information.
- CRS[9] matrix format is used to store the stiffness matrix.
- SEM is assembled element-wise.
- AES-FEM is assembled node-wise.
- HIFIR[10] preconditioned GMRES is used to solve the linear system.

[8] Dyedov et al., *Eng. Comput.* (2015)
[9] Bank and Douglas, *Adv. Comput. Math.* (1993).
[10] Q. Chen and Jiao, *ACM Trans. Math. Softw.* (2022).

ApSEM Flowchart

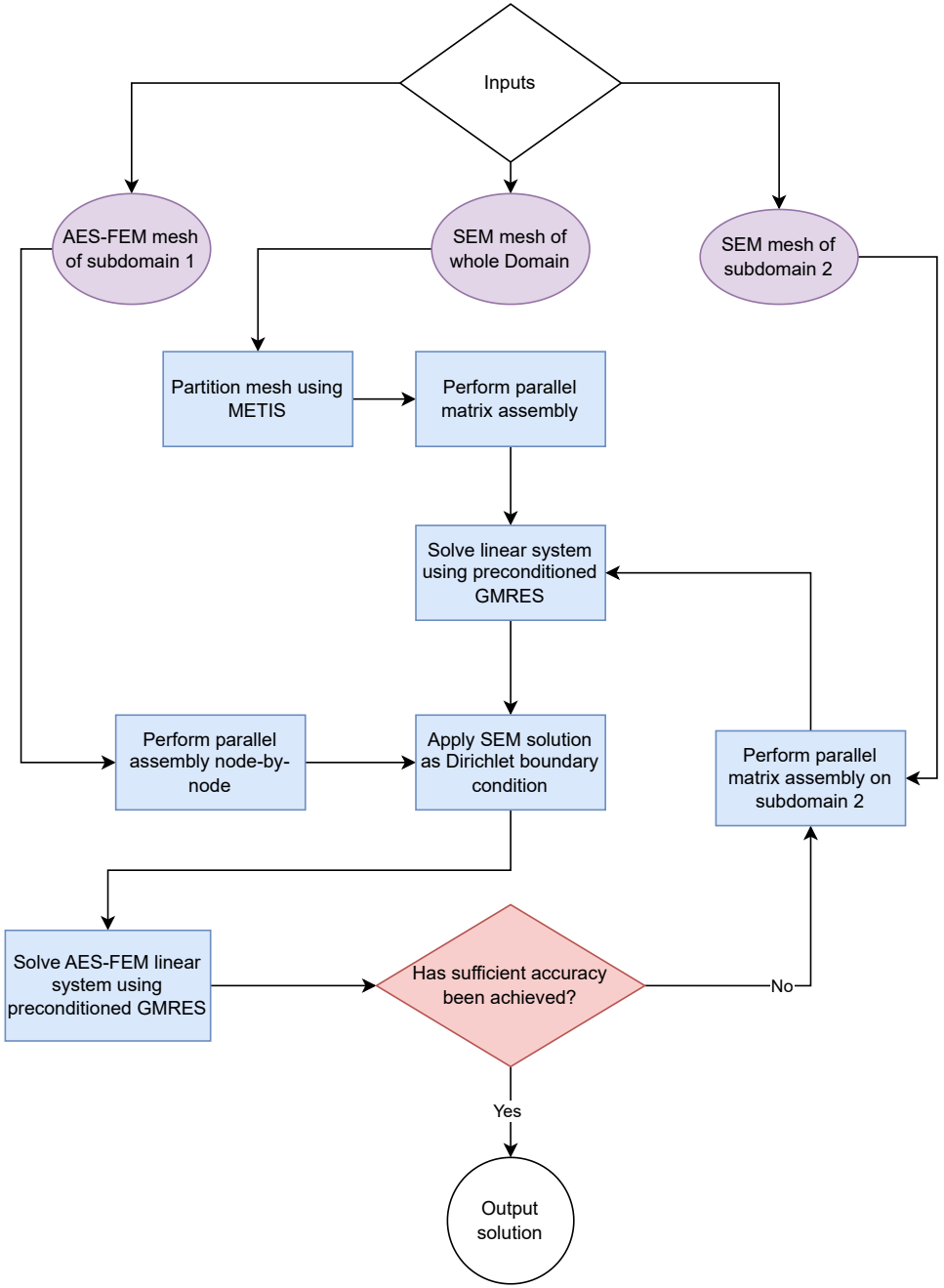

Outline

Test Problem

- We solve the convection-diffusion equation:

$$\begin{aligned} -\Delta u + \boldsymbol{v} \cdot \boldsymbol{\nabla} u &= f \quad \text{in } \Omega, \\ u &= u_D \quad \text{on } \Gamma_D, \\ \partial_{\boldsymbol{n}} u &= u_N \quad \text{on } \Gamma_N. \end{aligned}$$

- We utilize the method of manufactured solutions in 3D and compute f, u_D, and u_N from the exact solution $uu = \sin(10x)\cos(10y)\sin(10z) + xyz$ and $\boldsymbol{v} = [x, y, -2z]$.
- We conduct the tests using a unit box centered at $(0.5, 0.5)$ with a spherical hole.

Domain Used in Tests

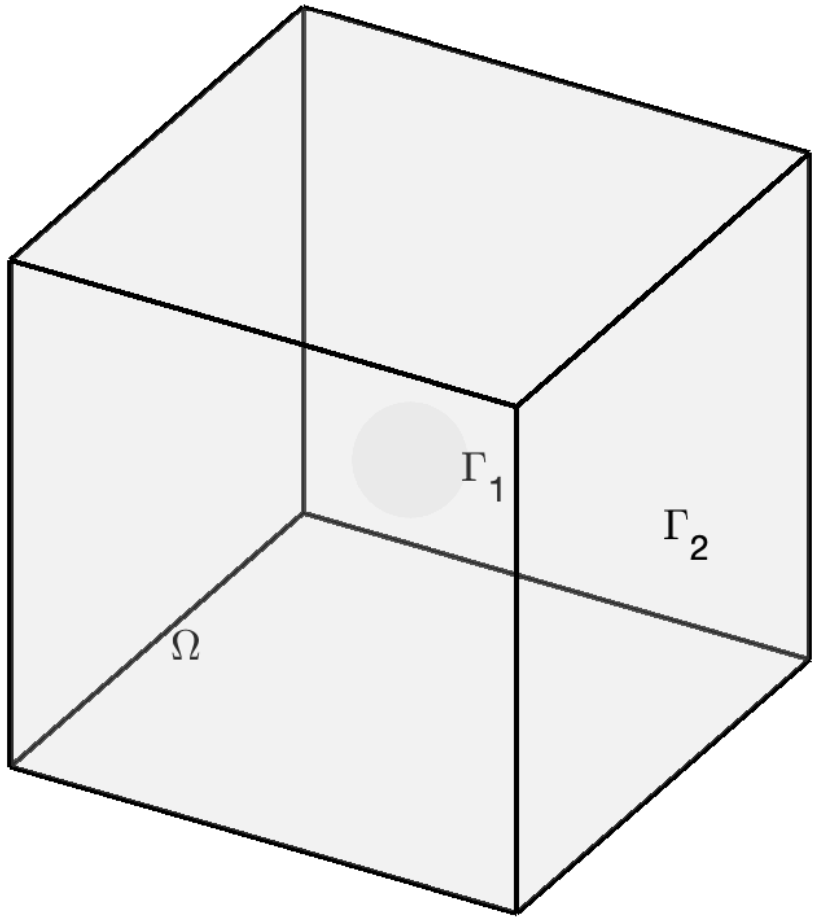

Figure: Domain used in 3D tests. Neumann or Dirichlet boundary conditions are applied to interior boundary Γ_1; Dirichlet boundary conditions are applied to exterior boundary Γ_2.

Measuring Superconvergence

- To demonstrate superconvergence, we measure the errors in ℓ_2 norm.
- Since the elements near the boundaries are quite irregular, we compute the convergence rate based on the number of degrees of freedom (dof), i.e.,

$$\text{convergence rate} = \frac{-\log\left(\frac{\text{error of fine mesh}}{\text{error of coarse mesh}}\right)}{\log\left(\sqrt[d]{\frac{\text{dof in fine mesh}}{\text{dof in coarse mesh}}}\right)},$$

where $d = 3$ is the topological dimension of the mesh.

Comparison of Error with Neumann Boundary Conditions

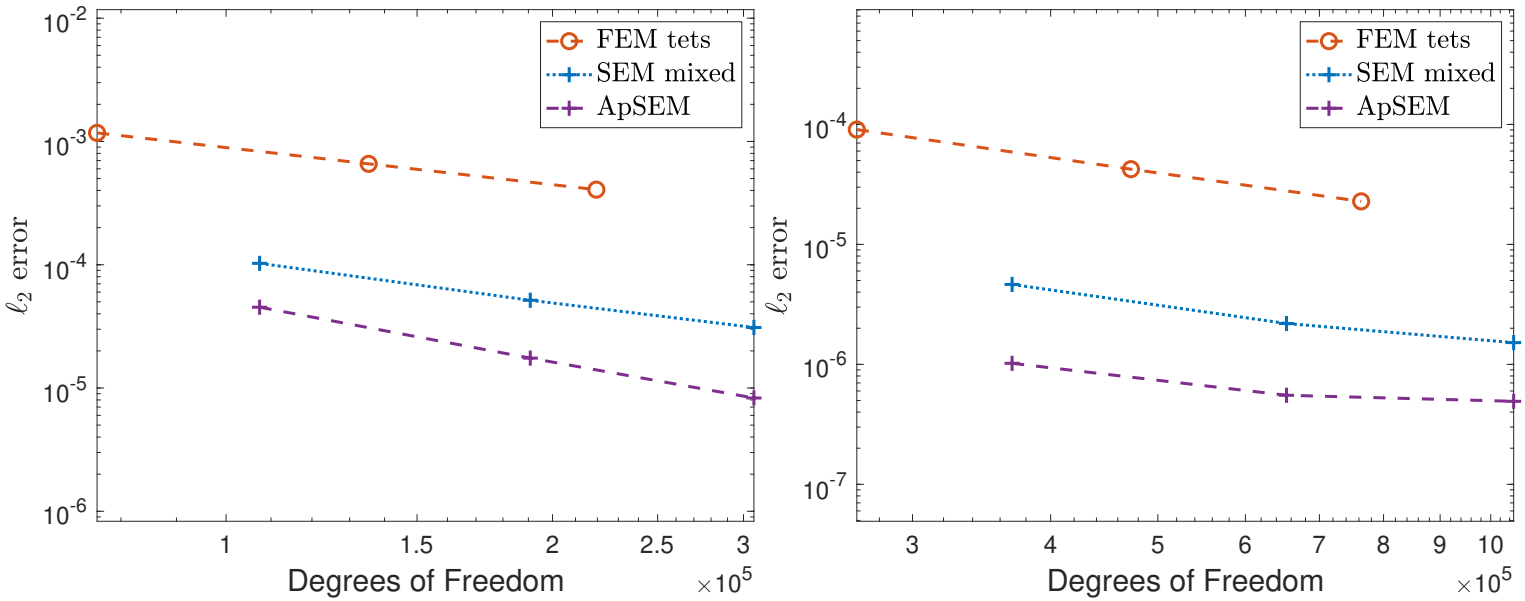

(a) Quadratic spherical hole

(b) Cubic spherical hole

Comparison of Error with Neumann Boundary Conditions

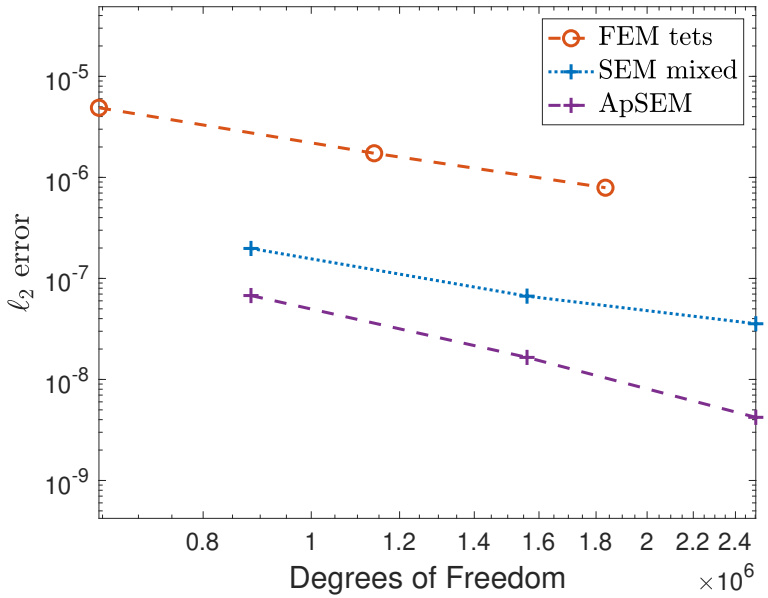

(c) Quartic spherical hole

Comparison of Error with Neumann Boundary Conditions

Table: A comparison of the error of different methods for the convection-diffusion equation on the spherical hole domain with Dirichlet boundary conditions on the cube and Neumann boundary conditions on the spherical hole and quadratic FEM, SEM, and ApSEM. The convergence rate is showed in parenthases.

Mesh Refinement Level	FEM Tets	SEM Mixed	ApSEM
1	1.17e-03	1.03e-04	4.52e-05
2	6.58e-04 (3.01)	5.15e-05 (3.60)	1.75e-05 (4.96)
3	4.07e-04 (2.99)	3.10e-05 (3.21)	8.30e-06 (4.71)

Comparison of Error with Neumann Boundary Conditions

Table: A comparison of the error of different methods for the convection-diffusion equation on the spherical hole domain with Dirichlet boundary conditions on the cube and Neumann boundary conditions on the spherical hole and cubic FEM, SEM, and ApSEM. The convergence rate is showed in parenthases.

Mesh Refinement Level	FEM Tets	SEM Mixed	ApSEM
1	9.06e-05	4.64e-06	1.02e-06
2	4.24e-05 (3.99)	2.19e-06 (3.94)	5.52e-07 (3.22)
3	2.28e-05 (3.87)	1.52e-06 (2.33)	4.92e-07 (0.74)

Comparison of Error with Neumann Boundary Conditions

Table: A comparison of the error of different methods for the convection-diffusion equation on the spherical hole domain with Dirichlet boundary conditions on the cube and Neumann boundary conditions on the spherical hole and quartic FEM, SEM, and ApSEM. The convergence rate is showed in parenthases.

Mesh Refinement Level	FEM Tets	SEM Mixed	ApSEM
1	4.89e-06	1.98e-07	6.77e-08
2	1.73e-06 (5.48)	6.68e-08 (5.72)	1.65e-08 (7.42)
3	7.90e-07 (4.94)	3.56e-08 (4.00)	4.22e-09 (8.68)

Comparison of Error with Dirichlet Boundary Conditions

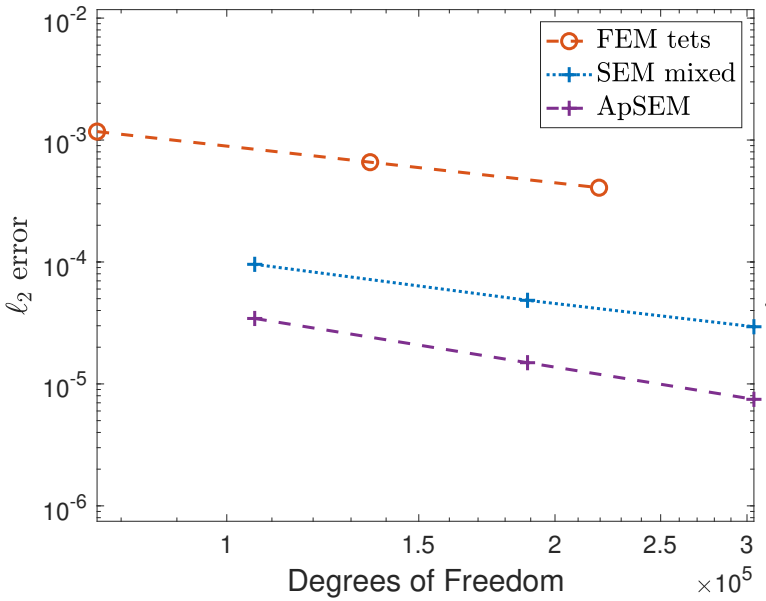

(a) Quadratic spherical hole

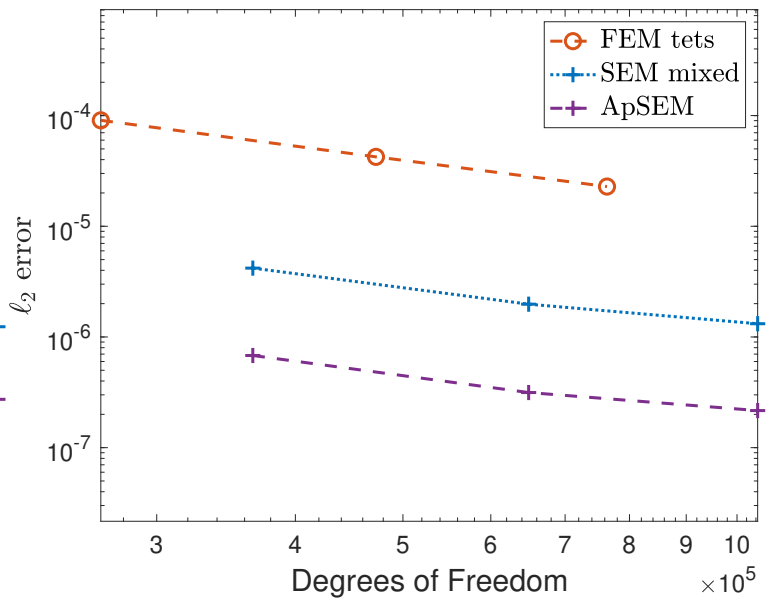

(b) Cubic spherical hole

Comparison of Error with Dirichlet Boundary Conditions

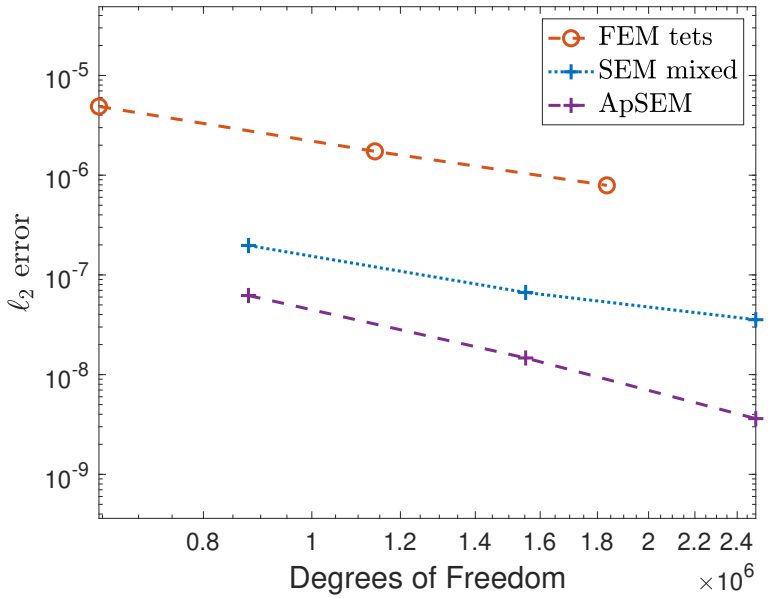

(c) Quartic spherical hole

Comparison of Error with Dirichlet Boundary Conditions

Table: A comparison of the error of different methods for the convection-diffusion equation on the spherical hole domain with Dirichlet boundary conditions and quadratic FEM, SEM, and ApSEM. The convergence rate is showed in parenthases.

Mesh Refinement Level	FEM Tets	SEM Mixed	ApSEM
1	1.17e-03	9.57e-05	3.44e-05
2	6.58e-04 (3.01)	4.85e-05 (3.54)	1.49e-05 (4.35)
3	4.07e-04 (2.99)	2.94e-05 (3.13)	7.48e-06 (4.34)

Comparison of Error with Dirichlet Boundary Conditions

Table: A comparison of the error of different methods for the convection-diffusion equation on the spherical hole domain with Dirichlet boundary conditions and cubic FEM, SEM, and ApSEM. The convergence rate is showed in parenthases.

Mesh Refinement Level	FEM Tets	SEM Mixed	ApSEM
1	9.06e-05	4.19e-06	6.80e-07
2	4.24e-05 (3.99)	1.98e-06 (3.93)	3.15e-07 (4.04)
3	2.28e-05 (3.87)	1.32e-06 (2.57)	2.16e-07 (2.37)

Comparison of Error with Dirichlet Boundary Conditions

Table: A comparison of the error of different methods for the convection-diffusion equation on the spherical hole domain with Dirichlet boundary conditions and quartic FEM, SEM, and ApSEM. The convergence rate is showed in parenthases.

Mesh Refinement Level	FEM Tets	SEM Mixed	ApSEM
1	4.89e-06	1.97e-07	6.21e-08
2	1.73e-06 (5.48)	6.67e-08 (5.70)	1.47e-08 (7.59)
3	7.90e-07 (4.94)	3.55e-08 (3.99)	3.62e-09 (8.87)

Impact of Mesh Quality

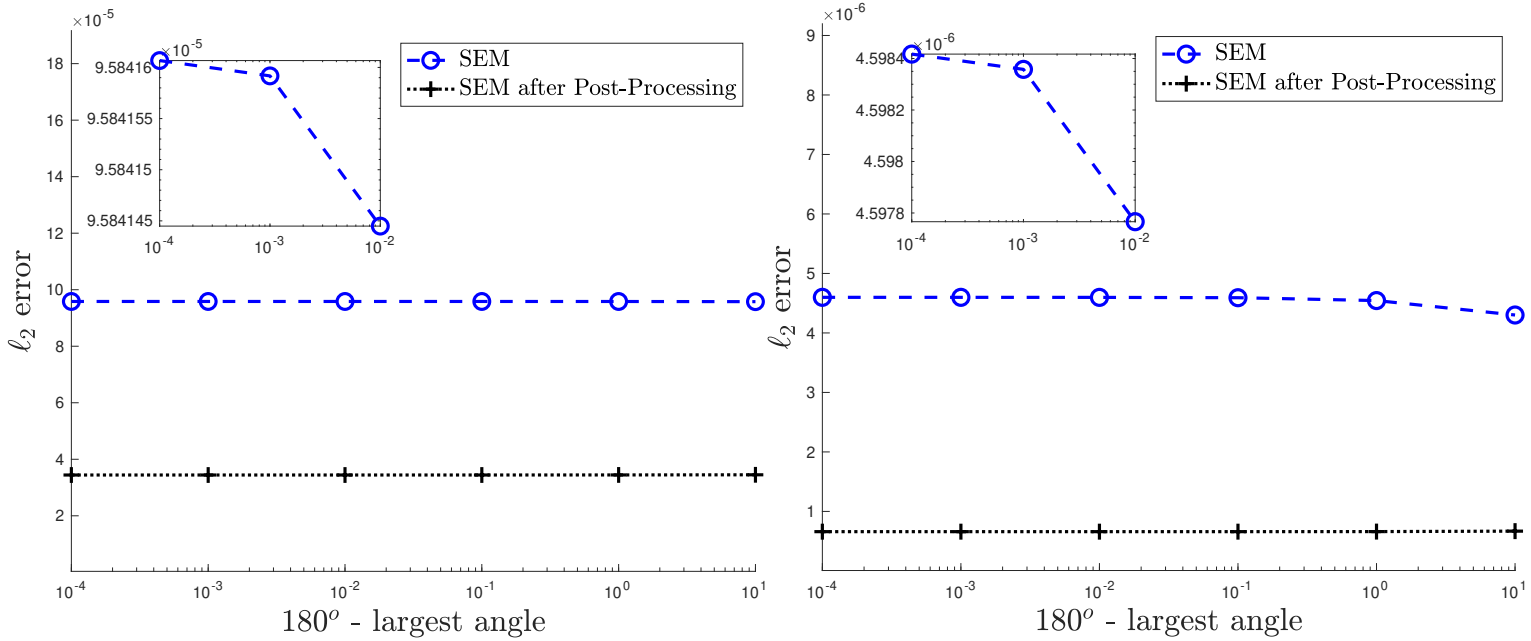

(a) Quadratic

(b) Cubic

Impact of Mesh Quality

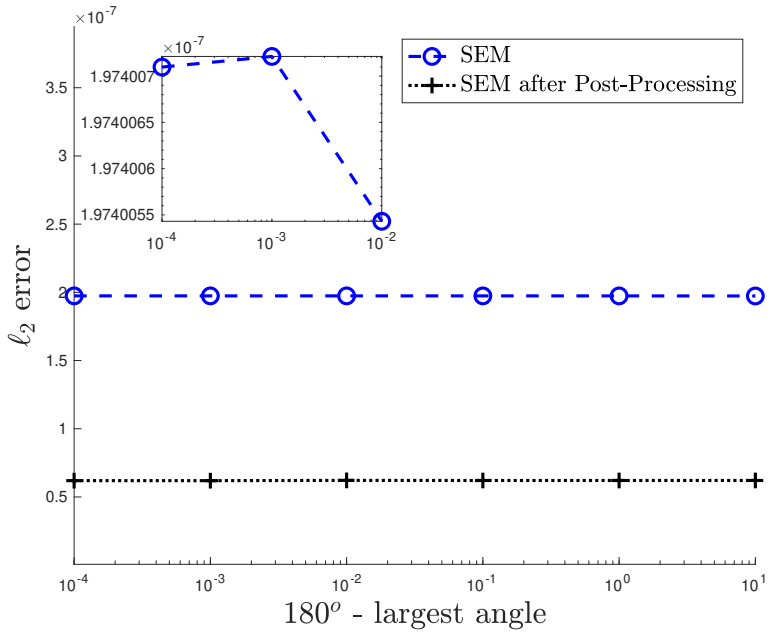

(c) Quartic

Timing Results for Neumann Boundary Conditions

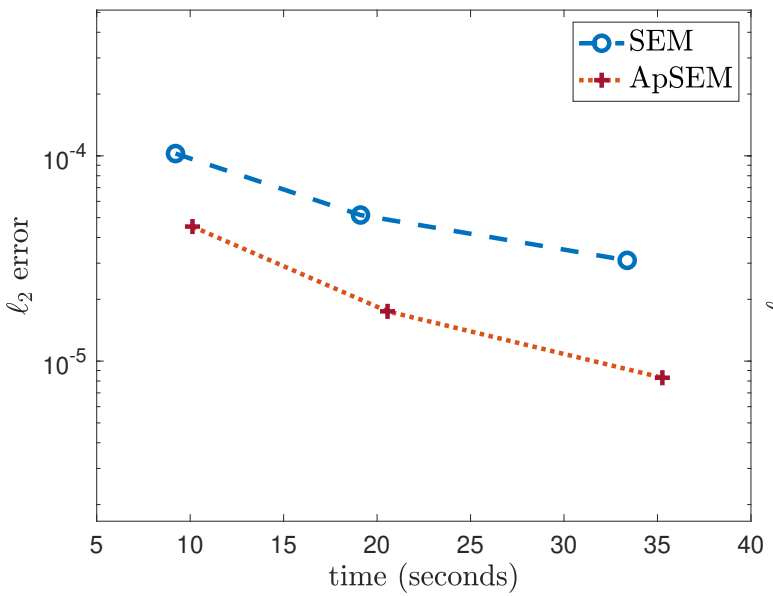

(a) Quadratic spherical hole

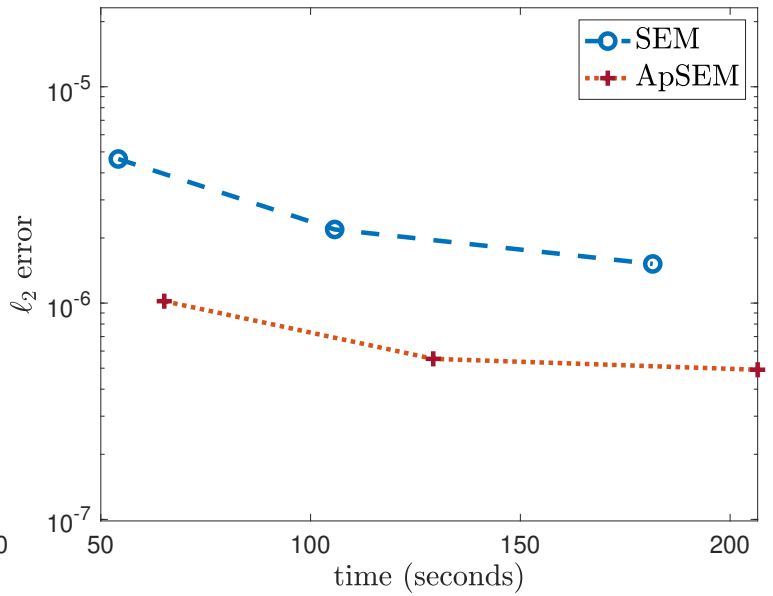

(b) Cubic spherical hole

Timing Results for Neumann Boundary Conditions

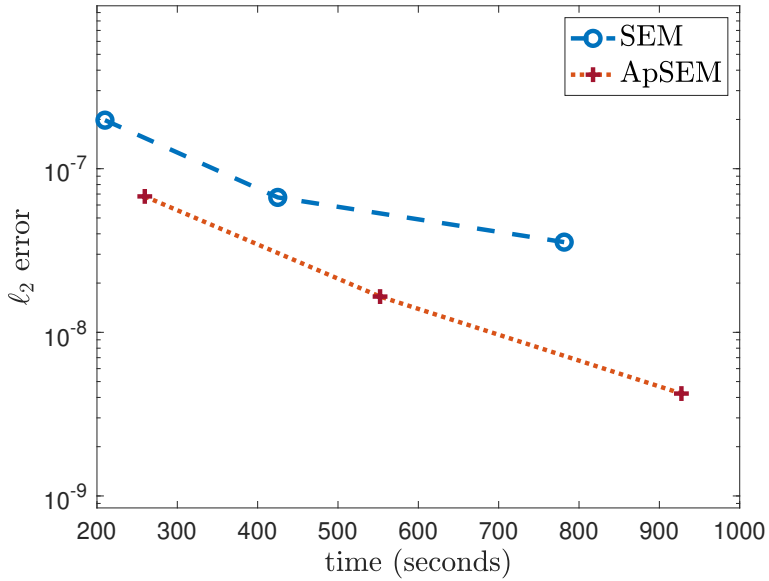

(c) Quartic spherical hole

Timing Results for Neumann Boundary Conditions

Table: A table comparing the time taken to assemble and solve the linear system for the Neumann problem using SEM and AES-FEM as the mesh is refined. The total percentage of time taken by AES-FEM is also shown.

Degree	Mesh Refinement Level	SEM		AES-FEM		Total % of AES-FEM
		assembly	solve	assembly	solve	
2	1	0.33 (3.25%)	8.89 (87.78%)	0.27 (2.70%)	0.63 (6.27%)	8.97%
	2	0.53 (2.59%)	18.58 (90.37%)	0.43 (2.07%)	1.02 (4.96%)	7.04%
	3	0.80 (2.26%)	32.58 (92.41%)	0.50 (1.41%)	1.39 (3.93%)	5.33%
3	1	2.85 (4.37%)	51.32 (78.80%)	1.76 (2.70%)	9.20 (14.13%)	16.83%
	2	4.84 (3.74%)	100.91 (78.08%)	2.84 (2.19%)	20.66 (15.98%)	18.18%
	3	7.65 (3.71%)	173.90 (84.19%)	3.17 (1.53%)	21.84 (10.57%)	12.11%
4	1	18.23 (7.02%)	191.72 (73.87%)	3.50 (1.35%)	46.07 (17.75%)	19.10%
	2	33.12 (6.00%)	391.89 (70.95%)	5.33 (0.96%)	122.03 (22.09%)	23.06%
	3	57.75 (6.23%)	723.81 (78.04%)	6.08 (0.66%)	139.82 (15.08%)	15.73%

Timing Results for Dirichlet Boundary Conditions

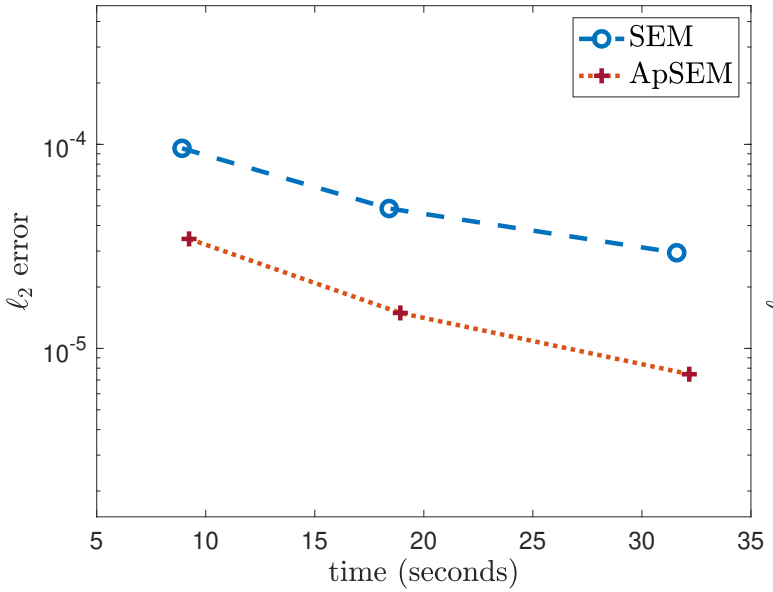

(a) Quadratic

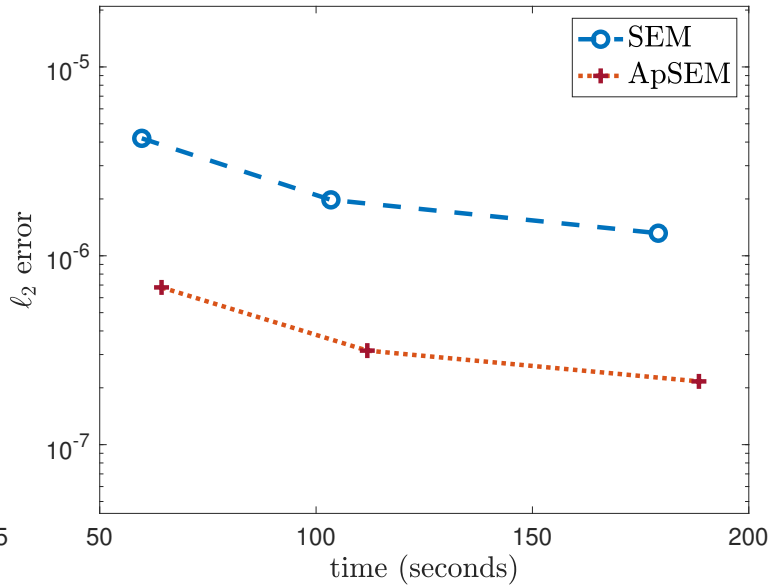

(b) Cubic

Timing Results for Dirichlet Boundary Conditions

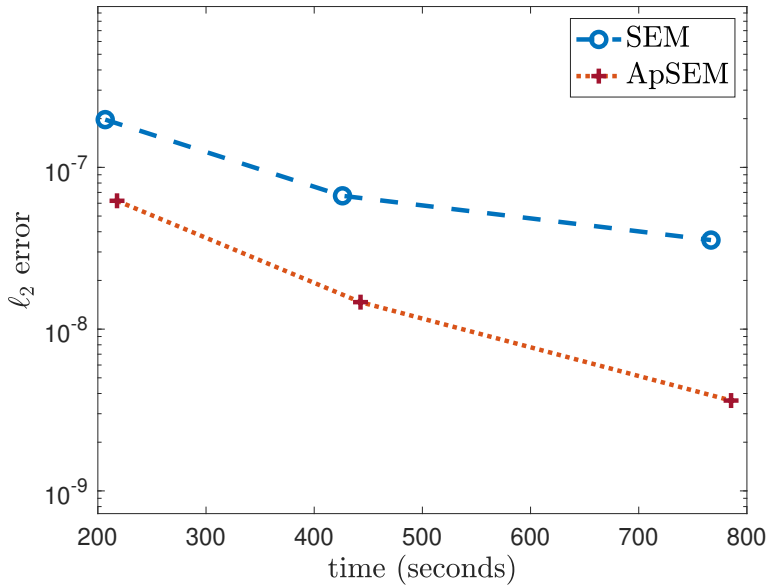

(c) Quartic

Timing Results for Dirichlet Boundary Conditions

Table: A table comparing the time taken to assemble and solve the linear system for the Dirichlet problem using SEM and AES-FEM as the mesh is refined. The total percentage of time taken by AES-FEM is also shown.

Degree	Mesh Refinement Level	SEM		AES-FEM		Total % of AES-FEM
		assembly	solve	assembly	solve	
2	1	0.32 (3.47%)	8.59 (93.05%)	0.01 (0.12%)	0.31 (3.36%)	3.48%
	2	0.51 (2.68%)	17.90 (94.62%)	0.01 (0.08%)	0.50 (2.63%)	2.71%
	3	0.76 (2.36%)	30.84 (95.85%)	0.02 (0.05%)	0.56 (1.74%)	1.79%
3	1	7.27 (11.30%)	52.45 (81.59%)	0.07 (0.10%)	4.50 (7.00%)	7.11%
	2	4.80 (4.29%)	98.63 (88.19%)	0.11 (0.09%)	8.31 (7.43%)	7.52%
	3	7.56 (4.01%)	171.53 (91.01%)	0.12 (0.06%)	9.27 (4.92%)	4.98%
4	1	18.12 (8.32%)	188.69 (86.67%)	0.15 (0.07%)	10.76 (4.94%)	5.01%
	2	31.36 (7.08%)	394.81 (89.16%)	0.23 (0.05%)	16.42 (3.71%)	3.76%
	3	49.73 (6.33%)	717.07 (91.31%)	0.26 (0.03%)	18.29 (2.33%)	2.36%

Outline

Complex Geometries in Meshing Workflow

- Our workflow handles general geometries.
- We must test ApSEM with complex shapes like turbine blades or wings.
- Integrating these into ApSEM is ongoing, but *h*-GR extension is simple.
- Main challenges:
  - Curvature definition: Use minimum radius for smooth surfaces, normal direction difference for corners.
  - 3D scalability: Surface intersections can define multiple target edge lengths.
  - Handling domains for which we lack an explicit parameterization.

Geometric Reconstruction and Node Positioning

- Use Hermite Style Reconstruction (HSR)[11] for local geometry.
- HSR uses Weighted Least Squares for local patches.
- Divide sharp corners into patches or use feature-aware HSR.
- Project high-order nodes onto the curved surface.
- Orthogonal projection results in stable, smooth elements.
- Given a triangle T_e and its WLS polynomial $WLS(T_e)$, find $u \in WLS(T_e) \subset \mathbb{R}^2$ for point p such that:

$$(p - WLS(u)) \cdot \nabla WLS(u) = 0.$$

- Use Newton-Raphson to find this point.
- This method efficiently projects points onto a curved surface.

[11] Li et al., *Eng. Comput.* (2021).

NACA 2412 Airfoil Meshing with *h*-GR

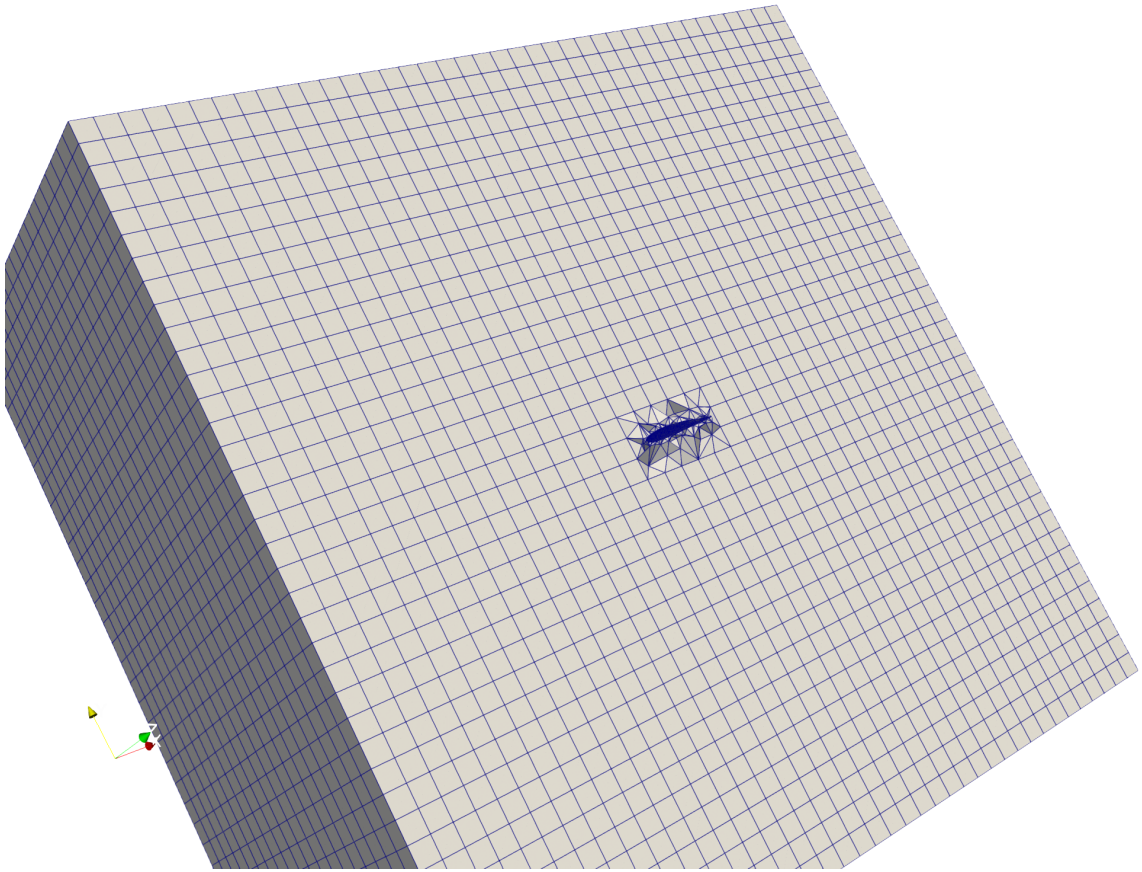

Figure: Full linear mixed mesh for the NACA 2412 airfoil with *h*-GR. The curved geometric hole is very small compared to the entire domain.

Close-up View of NACA 2412 Airfoil Meshing with *h*-GR

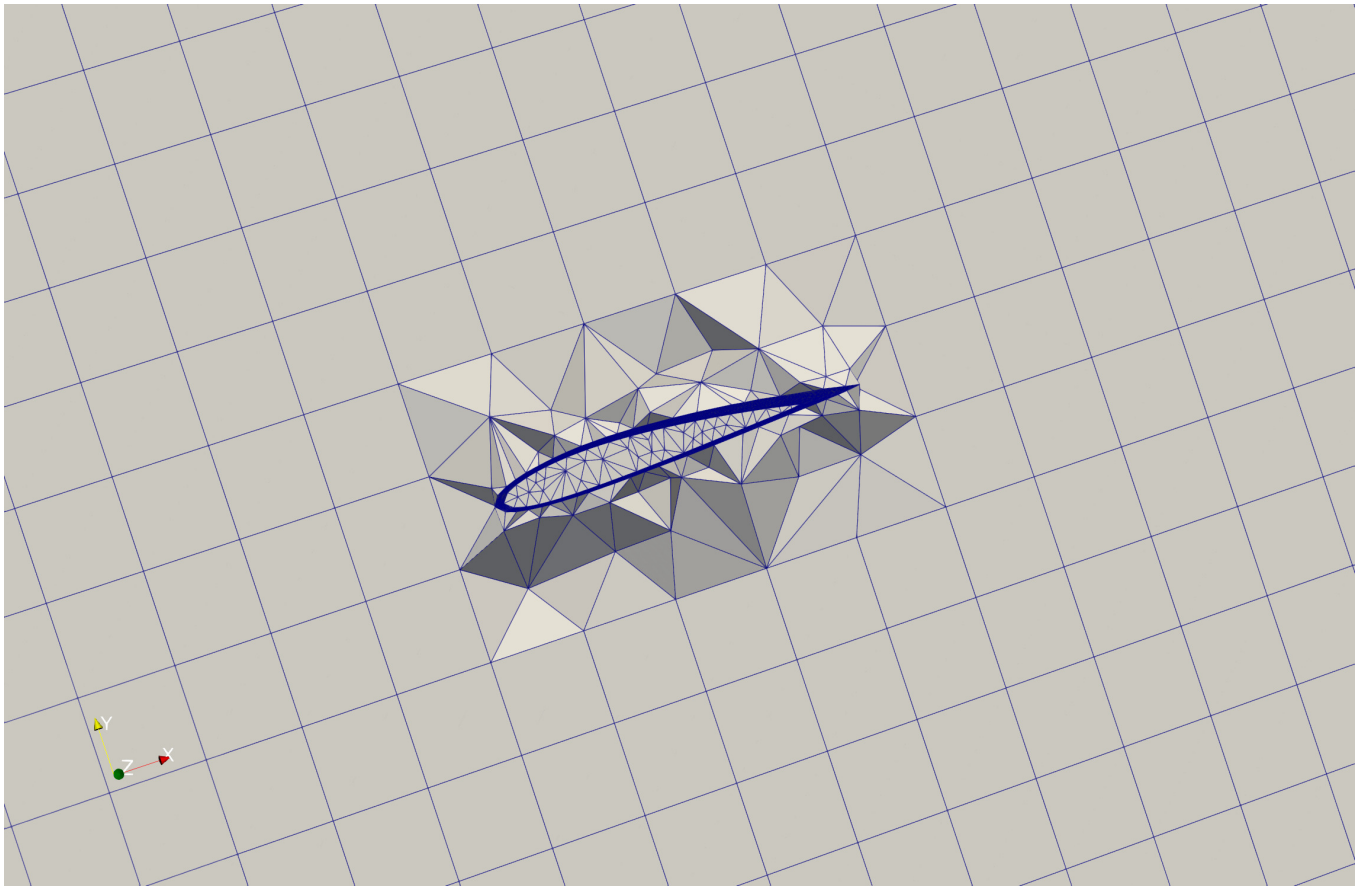

Figure: Close-up linear mixed mesh for the NACA 2412 airfoil with *h*-GR.

Outline

Conclusion

- Novel strategy enhances SEM accuracy over curved domains.
- New post-processing method, ApSEM, achieves accuracy parity between different element types.
- Demonstrated SEM superconvergence over curved domains in 2D and 3D.
- Techniques boost solution accuracy by 1–2 orders of magnitude.
- Accuracy improvement is shape quality independent.
- Strategy relaxes element-shape requirements near boundaries.
- ApSEM is more cost-effective than standard SEM.

Future Work

- Superconvergence for Complex Geometries in 3D:
  - Use local geometric reconstructions in Li. et al.[12] to handle complex geometries.
  - Project nodes onto curved surfaces using orthogonal projection.
- Extension to other PDEs:
  - Nonlinear solid mechanics.
  - Parabolic PDEs.
  - Fluid dynamics.

[12] Li et al., *Eng. Comput.* (2021).

Thank you

To my advisor Dr. Jiao,
To all past and present members of the research group,
To the thesis committee,
To my friends and family,

Thank you!

Difference between L^2-Norm and ℓ^2-norm

- The L^2-norm, also known as the Euclidean norm, is used in the context of function spaces. It is defined for a solution u as:

$$\|u\|_{L^2} = \sqrt{\int |u(x)|^2 dx}$$

- The ℓ_2-norm, on the other hand, is used in the context of the solutions at nodes. It is defined as:

$$\|u\|_{\ell_2} = \sqrt{\sum |u_i|^2}$$

- When measuring superconvergence for SEM we use the ℓ_2-norm as the L^2-norm is dominated by interpolation error

Element Orthogonality Analysis (EOA)

- EOA[13] is a method for superconvergence analysis in PDEs.
- It constructs an orthogonal polynomial interpolant of the PDE solution u that is close to the FEM solution u_h.
- The finite element solution u_h satisfies:

$$a(u - u_h, v) = 0.$$

- Define the one-dimensional master element $\tau(\xi) = (-1, 1)$.
- *Legendre* polynomials l_n are derived as:

$$l_n(\xi) = \frac{1}{2^n n!} \frac{d^n}{d\xi^n}(\xi^2 - 1)^n.$$

- *Lobatto* polynomials are obtained by integrating over ξ:

$$\mathcal{L}_{n+1}(\xi) = \frac{1}{2^n n!} \frac{d^{n-1}}{d\xi^{n-1}}(\xi^2 - 1)^n.$$

[13] C. Chen, *Int. J. Numer. Anal. Model.* (2005).

Superconvergence of Lobatto Points in SEM

- Represent the PDE solution u as an orthogonal expansion over $\tau(\xi)$:

$$u(\xi) = \sum_{i=0}^{\infty} A_i \mathcal{L}_i(\xi),$$

$$u_k(\xi) = \sum_{i=0}^{k} A_i \mathcal{L}_i(\xi). \tag{1}$$

- Superconvergence results from the residual of the expansion:

$$\begin{aligned} R = u - u_n &= \sum_{i=k+1}^{\infty} A_i \mathcal{L}_i(\xi) \\ &= A_{k+1} \mathcal{L}_{k+1}(\xi) + \mathcal{O}(h^{k+2}). \end{aligned} \tag{2}$$

Numerical Demonstration: Loss of Superconvergence

- A numerical study on cubic spectral elements supports the claim that orthogonality loss leads to superconvergence loss.
- We created square elements in the unit box $[0, 1] \times [0, 1]$ and perturbed the nodes to violate orthogonality. This perturbation was limited to the interior nodes and did not exceed 5%.
- The convergence rate drops to $\mathcal{O}(h^4)$ for both homogeneous and inhomogeneous boundary conditions.
- Superconvergence loss is a gradual process that worsens with increasing orthogonality deviation, indicating an error that grows as the deviation expands.

Numerical Demonstration: Loss of Superconvergence

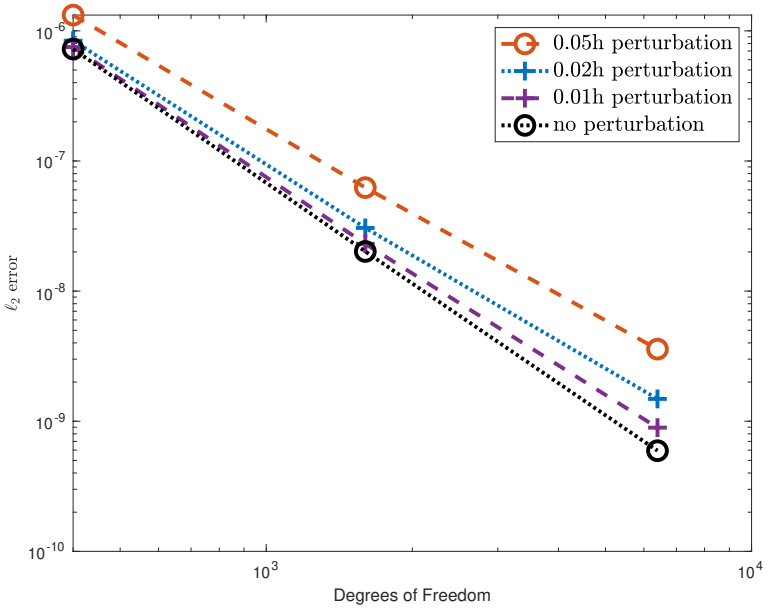

Figure: Homogeneous boundary conditions

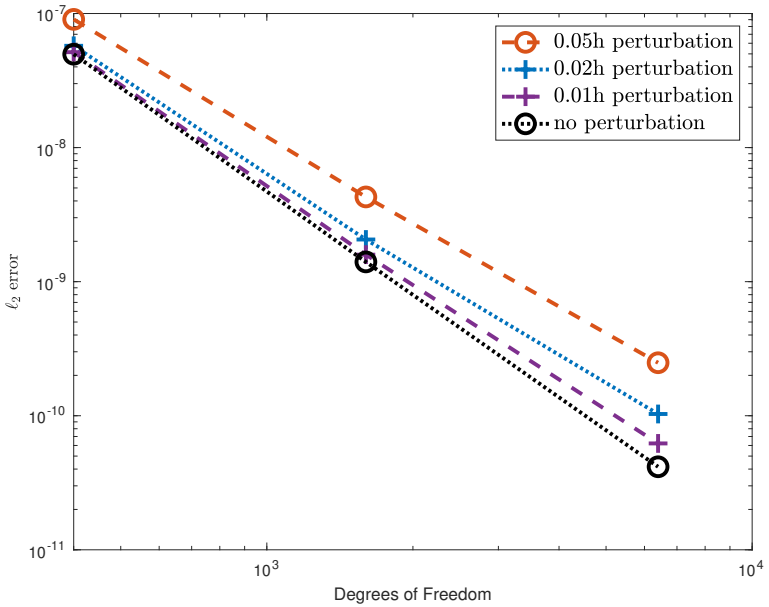

Figure: Inhomogeneous boundary conditions

Numerical Demonstration: Loss of Superconvergence

Table: Homogeneous boundary conditions with small perturbations in nodal positions.

$0.05h$ perturbation	$0.02h$ perturbation	$0.01h$ perturbation	no perturbation
1.29e-06	8.28e-07	7.54e-07	7.25e-07
6.29e-08	3.01e-08	2.31e-08	2.02e-08
3.58e-09 (4.25)	1.46e-09 (4.57)	8.89e-10 (4.86)	5.94e-10 (5.12)

Numerical Demonstration: Loss of Superconvergence

Table: Cubic spectral elements with inhomogeneous boundary conditions and small perturbations in nodal positions.

$0.05h$ perturbation	$0.02h$ perturbation	$0.01h$ perturbation	no perturbation
9.10e-08	5.58e-08	5.14e-08	4.97e-08
4.31e-09	2.08e-09	1.60e-09	1.40e-09
2.53e-10 (4.24)	1.01e-10 (4.55)	6.24e-11 (4.84)	4.16e-11 (5.11)

Lemma: Orthogonality and Superconvergence in Spectral Elements

Lemma

Let τ be an n-dimensional tensor-product element without curved facets. If τ's geometry deviates from orthogonality, superconvergence in the ℓ_2 sense is lost for the spectral element method assuming no other error cancellation mechanisms are present.

Proof: Part 1

Consider an element τ that, despite potentially being of high order, possesses a linear geometry due to the absence of curved facets. The basis functions employed for interpolating points within this element are thus the tensor-products of n one-dimensional linear basis functions over the 1D reference element $[0, 1]$, denoted as $\mathbb{P}_1^1(\boldsymbol{\xi}) = \{1 - \boldsymbol{\xi}, \boldsymbol{\xi}\}$:

$$\mathbb{Q}_1^n = \bigotimes_{i=1}^{n} \mathbb{P}_1^1(\xi_i).$$

Proof: Part 2

The interpolation on τ is defined in the conventional manner as

$$\boldsymbol{x}(\xi_1, \xi_2, ..., \xi_n) = \sum_{i=1}^{n} \boldsymbol{x}_i \phi_i(\xi_1, \xi_2, ..., \xi_n),$$

where $\boldsymbol{x}_i$ represents the knot points of the element τ and ϕ_i is a basis function in $\mathbb{Q}_1^n$.

Proof: Part 3

In the event that the geometric configuration of the element is orthogonal, the interpolation in each dimension can be decoupled and reduced to a straightforward interpolation in one dimension. This is achieved by utilizing the components of the two corner nodes of the element. Formally, this can be expressed as:

$$\boldsymbol{x}_d(\xi_d) = (1 - \xi_d)\boldsymbol{x}_{d_1} + \xi_d \boldsymbol{x}_{d_2},$$

where x_d denotes the dth component of $\boldsymbol{x}$, and $\boldsymbol{x}_{d_1}$ and $\boldsymbol{x}_{d_2}$ represent the dth components of the two corner nodes of τ.

Proof: Part 4

The standard interpolation can be represented as a decoupled formulation, albeit with an associated error term. This can be formally expressed as:

$$\boldsymbol{x}_d(\xi_d) = (1 - \xi_d)\boldsymbol{x}_{d_1} + \xi_d \boldsymbol{x}_{d_2} + \mathcal{O}(\boldsymbol{\xi}^2).$$

This error term is incorporated into the mapping of the residual equation 2, which results in the residual equation deviating from zero. This deviation subsequently impinges on the convergence rate of the spectral element method, leading to the loss of superconvergence. It is noteworthy that the error term is of order $\mathcal{O}(\boldsymbol{\xi}^2)$, implying that it escalates with an increase in the divergence from orthogonality.

Algorithm Obtain 3D stencil for a given node

1: Initialize current ring size rs to be 0
2: Initialize desired ring size drs to be the original desired ring size ogs
3: **while** $rs < drs$ **do**
4: **if** $drs - rs = 1/3$ **then**
5: Expand by $1/3$ ring
6: $rs \leftarrow rs + 1/3$
7: **else if** $drs - rs = 2/3$ **then**
8: Expand by $2/3$ ring
9: $rs \leftarrow rs + 2/3$
10: **else**
11: Expand by full ring
12: $rs \leftarrow rs + 1$
13: **end if**
14: **if** any vertex in the recently computed stencil is on the boundary **then**
15: $drs \leftarrow ogs + (ogs - rs)$
16: **end if**
17: **if** $rs \geq drs$ and number of vertices in stencil $<$ desired number of vertices in stencil **then**
18: $drs \leftarrow drs + 1$
19: **end if**
20: **end while**

Curvature-Based h-GR to 3D

- In this context, we can use the minimum radius of curvature, which is the reciprocal of the maximum curvature, to control the edge length.
- Given a smooth parametric surface $S(u, v) \in \mathbb{R}^2 \to \mathbb{R}^3$, let $\boldsymbol{J}$ be the Jacobian matrix of S.
- The first fundamental matrix of S as $\boldsymbol{G} = \boldsymbol{J}^T \boldsymbol{J}$, and the second fundamental matrix is given by

$$\boldsymbol{B} = \begin{bmatrix} \hat{\boldsymbol{n}}^T S_{uu} & \hat{\boldsymbol{n}}^T S_{uv} \\ \hat{\boldsymbol{n}}^T S_{vu} & \hat{\boldsymbol{n}}^T S_{vv} \end{bmatrix},$$

  where $\hat{\boldsymbol{n}} = \frac{S_u \times S_v}{\|S_u \times S_v\|}$ are the unit normals.
- The principal curvatures are the eigenvalues of $\boldsymbol{W} = \boldsymbol{G}^{-1}\boldsymbol{B}$, and the minimum radius of curvature is the reciprocal of the maximum principal curvature.